



HAL
open science

Midlevel Cloud-Base Turbulence: Radar Observations and Models

L. Kantha, H. Luce, H. Hashiguchi

► **To cite this version:**

L. Kantha, H. Luce, H. Hashiguchi. Midlevel Cloud-Base Turbulence: Radar Observations and Models. Journal of Geophysical Research: Atmospheres, 2019, 124, pp.3223-3245. 10.1029/2018JD029479 . insu-03668093

HAL Id: insu-03668093

<https://insu.hal.science/insu-03668093>

Submitted on 14 May 2022

HAL is a multi-disciplinary open access archive for the deposit and dissemination of scientific research documents, whether they are published or not. The documents may come from teaching and research institutions in France or abroad, or from public or private research centers.

L'archive ouverte pluridisciplinaire **HAL**, est destinée au dépôt et à la diffusion de documents scientifiques de niveau recherche, publiés ou non, émanant des établissements d'enseignement et de recherche français ou étrangers, des laboratoires publics ou privés.

Copyright

JGR Atmospheres

RESEARCH ARTICLE

10.1029/2018JD029479

Key Points:

- Midlevel cloud-base turbulence observed by the MU radar in Shigaraki, Japan, during 2015 and 2016 is presented to show its ubiquitous nature
- A simple analytical model is presented for approximate estimation of turbulence parameters inside a MCT layer
- A one-dimensional second-moment closure-based turbulent mixing model is applied to an MCT event observed during 2015 and results compared to observations

Correspondence to:

L. Kantha,
 kantha@colorado.edu

Citation:

Kantha, L., Luce, H., & Hashiguchi, H. (2019). Midlevel cloud-base turbulence: Radar observations and models. *Journal of Geophysical Research: Atmospheres*, 124, 3223–3245. <https://doi.org/10.1029/2018JD029479>

Received 12 AUG 2018

Accepted 26 FEB 2019

Accepted article online 4 MAR 2019

Published online 23 MAR 2019

Author Contributions:

Conceptualization: L. Kantha, H. Luce

Formal analysis: L. Kantha

Investigation: H. Luce

Methodology: L. Kantha, H. Luce

Project administration: L. Kantha, H. Hashiguchi

Resources: H. Luce, H. Hashiguchi



Software: L. Kantha

Supervision: L. Kantha, H. Hashiguchi

Writing - original draft: L. Kantha

Writing - review & editing: L. Kantha, H. Luce

Midlevel Cloud-Base Turbulence: Radar Observations and Models

L. Kantha¹ , H. Luce², and H. Hashiguchi³ 

¹Department of Aerospace Engineering Sciences, University of Colorado Boulder, Boulder, CO, USA, ²Université de Toulon, Mediterranean Institute of Oceanography (MIO), UM 110, Toulon, France, ³Research Institute for Sustainable Humanosphere, Kyoto University, Kyoto, Japan

Abstract Midlevel Cloud-base Turbulence (MCT) caused by ice/snow precipitation from midlevel clouds falling into dry air below the cloud base and sublimating is investigated. MCT phenomena in the lower troposphere as revealed by the Middle and Upper atmosphere (MU) radar in Shigaraki, Japan, during the Shigaraki unmanned aerial vehicle and radar Experiment campaigns in the spring-summer of 2015 and 2016 are described. The MU radar was operated in a high-resolution (~20-m) range imaging mode and hence revealed the structure of these MCTs in great detail. These MCT layers grew to hundreds of meters in thickness, often reaching nearly 2,000 m in depth, lasting often for as much as 24 hr. A simple analytical model and a second-moment closure-based turbulent mixing model are used to estimate the levels of turbulence kinetic energy and its dissipation rate in the MCT layer and compare them to those measured by the MU radar. The study shows that MCT can give rise to moderate levels of turbulence of potential interest to aviation, confirming conclusions reached by earlier pioneering studies. However, to our knowledge, this important process has not received the attention it deserves by the atmospheric community so far, and therefore, it is the principal goal of this paper to not only present some observations and preliminary modeling results, but also redraw the attention of atmospheric scientists to this important process.

Plain Language Summary The free atmosphere above the planetary boundary layer is stably stratified, and therefore, turbulent mixing there is shear driven and occurs generally under the influence of stable density stratification. However, convective mixing can also occur there under certain conditions. When precipitating snow/ice particles fall below the cloud base of midlevel clouds, they can sublimate if the air column below the cloud is dry enough. The resulting cooling of the air column drives vigorous convection. This midlevel cloud-base turbulence process is the subject of this article.

1. Introduction

Convective mixing in the atmosphere is not confined merely to the atmospheric planetary boundary layer. Under appropriate conditions, vigorous convection can also take place in the interior of the moist troposphere. If the air immediately below the cloud base is dry enough, ice and snow particles falling from a midlevel cloud into the dry air below can initiate strong convection. The latent heat consumed by sublimation of ice/snow particles (and in some cases by evaporation of water particles) falling into the dry air below the cloud base cools the air, making it heavier, thus giving rise to convective instability. Unlike the convective boundary layer (CBL) studied intensively since the 1960s (e.g., Ball, 1960; Betts, 1973; Deardorff, 1970; Deardorff et al., 1969, 1980; Farmer, 1975; Kantha, 1980; Stull, 1973; Willis & Deardorff, 1974) and convection driven by cloud top cooling (Deardorff, 1976, 1980), very little attention has been paid to Midlevel Cloud-base Turbulence (MCT), the term coined by Kudo (2013) to describe this phenomenon, although Below Cloud-base Turbulence (BCT) may be better in some ways. Most investigations of mixing in the free troposphere have focused on mixing induced by Kelvin-Helmholtz (K-H) instabilities driven by wind shear in a stably stratified atmosphere. Possibility of convective mixing below a cloud base has largely been neglected.

Luce et al. (2010) were the first to present evidence of MCT from lidar and Middle and Upper atmosphere (MU) radar observations and Kudo (2013) was the very first to investigate MCT as the probable cause of moderate turbulence encountered by pilots under certain conditions during summer around Japan. Through numerical simulations, he showed that such turbulence was not caused by shear instability of the K-H type, but it was more likely due to precipitation below the bases of midlevel clouds, which

triggered Rayleigh-Taylor instability due to the sublimation of ice/snow particles and consequent cooling of the drier air mass below the cloud base. Kudo et al. (2015) followed up and presented observations of MCT during the Tanuki 2011 campaign at the MU radar site in Shigaraki, Japan, when some radiosondes launched during the campaign managed to sample the MCT, with the MU radar operating simultaneously in a high-resolution mode to provide vivid images of radar backscatter depicting the MCT structure. MU radar measurements of vertical velocities and turbulence kinetic energy (TKE) were presented along with in situ measurements by the sondes, and compared with numerical simulations.

Observations (Kudo et al., 2015) with the MU radar operating in high-resolution range imaging mode showed the MCT layer descending from ~ 8 km altitude (above ground level, AGL) at 16:00 LT on 25 September 2011 to ~ 3.2 km at 08:00 LT on September 26. The layer depth increased from ~ 700 m at 01:00 LT to $\sim 1,500$ m at 05:00 LT on 26 September. The radar measured up/downdrafts of up to ~ 2.3 m/s and TKE values of $0.63\text{--}0.85$ m^2/s^2 within the layer. A small stable gradient existed at the base of the MCT layer, without any significant shear. Kudo et al. (2015) ruled out K-H instability as the cause of the turbulent layer, although reliable shear measurements at the resolution needed could not be made. K-H instability is shear induced and can occur in stably stratified flows when the governing gradient Richardson number falls below 0.25. Numerical simulations using a 3-D regional model with an imbedded standard turbulence submodel and initialized using observational data from a radiosonde released at the MU radar site showed the formation of the MCT, with resulting TKE ranging between 0.3 and 0.75 m^2/s^2 within the layer and vertical velocities spanning -2 and $+2$ m/s, consistent with radar measurements.

MCT is likely to occur when a moist air mass is advected over a dry air mass, a condition quite common around Japan during the onset of spring-summer rainy period. Similar conditions can also be found elsewhere and so MCT is of interest, not only from the basic mixing process point of view but also from potential operational implications. In spite of the fact that the first article on MCT was published in 2010 (Luce et al., 2010) and was followed up by Kudo (2013) and Kudo et al. (2015), very little additional work has been done on MCT. Therefore, it is the primary goal of this paper to present and discuss MCT events observed during the 2015 and 2016 ShUREX (Shigaraki unmanned aerial vehicle [UAV] Radar Experiment) campaigns (Kantha et al., 2017) at the MU radar observatory and present a simple analytical model to describe the process as well as a second-moment closure-based turbulence model to simulate one of the events.

Virga is a related phenomenon. Virga precipitation is defined as the “wisps or streaks of water or ice particles falling out of a cloud but vaporizing before reaching the earth’s surface as precipitation,” according to Glickman (2000). It is especially prominent in arid regions such as the Sahara desert. Using ground radar, Rosenfeld and Mintz (1988) showed that all liquid water hydrometeors evaporate by 1.6 km below the cloud base if the rain rate is about 1 mm/hr. While considerable attention has been paid to virga precipitation because of its role in precipitation detection by passive microwave radiometers (Wang et al., 2018), not much is known about turbulence that could be generated below the cloud base by virga.

2. Materials and Methods

2.1. MCT Episodes During ShUREX 2015 and 2016

ShUREX 2015 and 2016 campaigns following the Tanuki 2011 campaign were similar except for the fact that for the very first time, UAVs, equipped with turbulence sensors, were flown in the vicinity of the MU radar to make in situ measurements of turbulence. The MU radar is a pulsed very high frequency (VHF) Doppler radar located at the Shigaraki MU Observatory (34.854061°N , 136.105606°E), Japan, 378 m above sea level. It is operated by the Research Institute for Sustainable Humanosphere of the Kyoto University (see Fukao et al., 1990). In standard mode, the radar operates at 46.5 MHz with a bandwidth of 3.5 MHz and a peak output power of 1 MW and consists of a 103-m-diameter array of 475 Yagi antennas that can be steered electronically. During the campaign, the radar was operated in range imaging mode using frequency diversity at vertical incidence (Luce et al., 2001). Owing to the radar parameter configuration used, resolution of a few tens of meters (typically ~ 20 m) was achieved for high signal-to-noise ratios, using the Capon processing method. More details of the radar and the campaigns can be found in Kantha et al. (2017) and Luce et al. (2018).

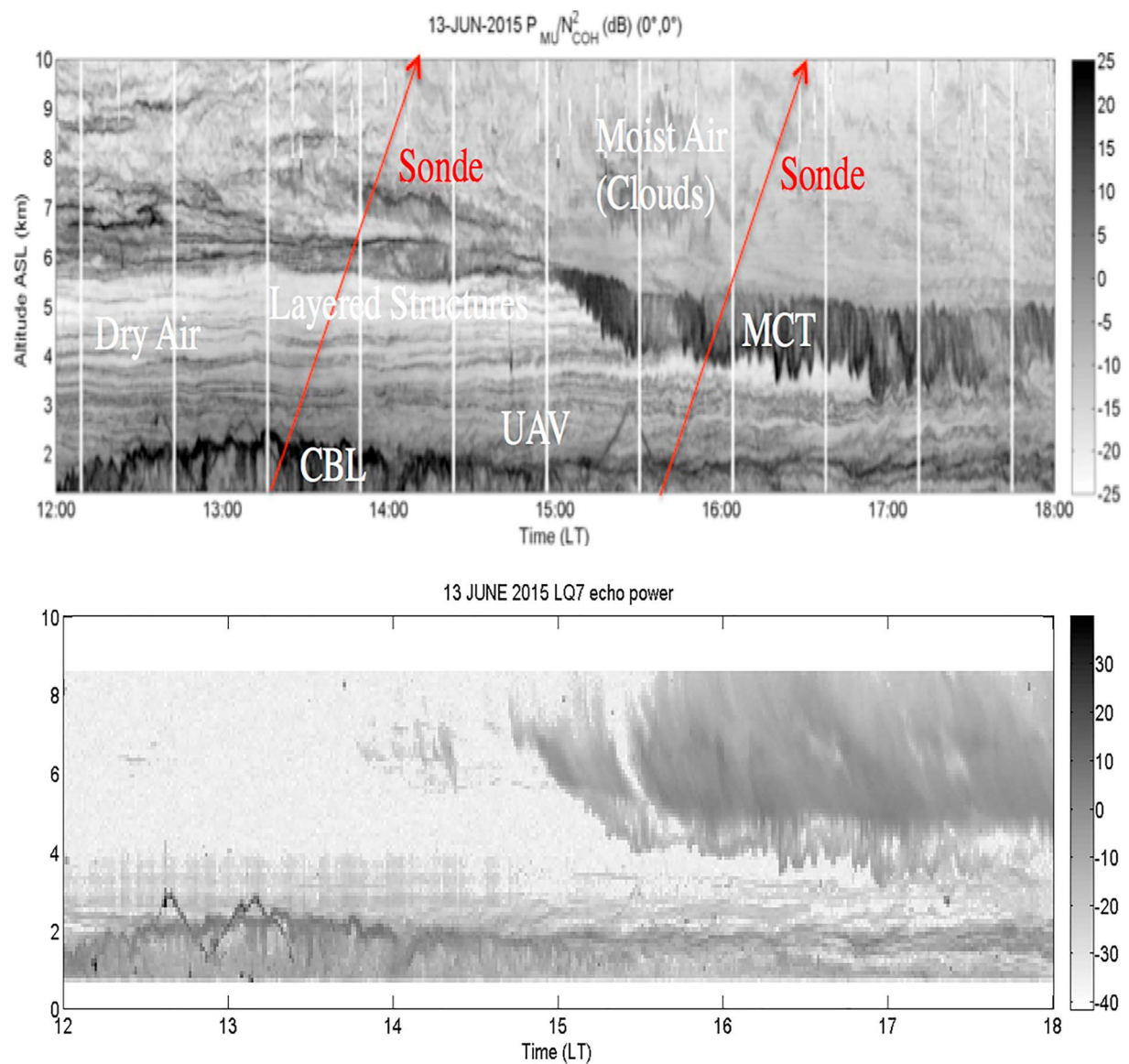


Figure 1. Top panel: Capon processed Middle and Upper atmosphere radar image on 13 June 2015, from 12:00 to 18:00 LT, with the radar operating in high-resolution (~20-m) range imaging mode. In addition to the MCT at altitudes between 3.5 and 5 km from 15:00 to 18:00 LT, the top of the CBL extending to 2 km above ground level can also be seen from 12:00 to 16:00 LT, before dissipating. UAV tracks can be seen as black lines around 13:00 LT and again after 15:00 LT. The radiosonde trajectories are shown as red lines. Bottom panel: The corresponding ultrahigh frequency radar image showing onset of precipitation in the cloud just before the onset of MCT at 14:40 LT. CBL and UAV tracks can also be seen. CBL = convective boundary layer; UAV = unmanned aerial vehicle; MCT = midlevel cloud-base turbulence.

We will first describe two of the outstanding MCT episodes observed during the two campaigns. The first one occurred on 13 June 2015, during the ShUREX 2015 campaign. The MU radar Capon image from 12:00 to 18:00 LT is shown in the upper panel of Figure 1. It can be seen that from 12:00 LT to just before 15:00 LT, the atmospheric column was characterized by a cloudy layer above an altitude (AGL) of roughly 6.4 km. Below the cloud base, there was a turbulent layer with a strong humidity gradient sheet at its bottom, with much drier air layer below the sheet. The cloud base descended to about 5.8 km AGL at 15:00 LT. Just after 15:00 LT, precipitation began to occur in the cloudy layer and an MCT layer developed immediately below the cloud base, wiping out the weak turbulent layer seen earlier. It grew very rapidly (almost linearly) to 1,350-m thickness in roughly 30 min, while the cloud base descended to about 5 km. It then remained at roughly the same thickness, while the cloud base also remained at about 5-km altitude. However, strong

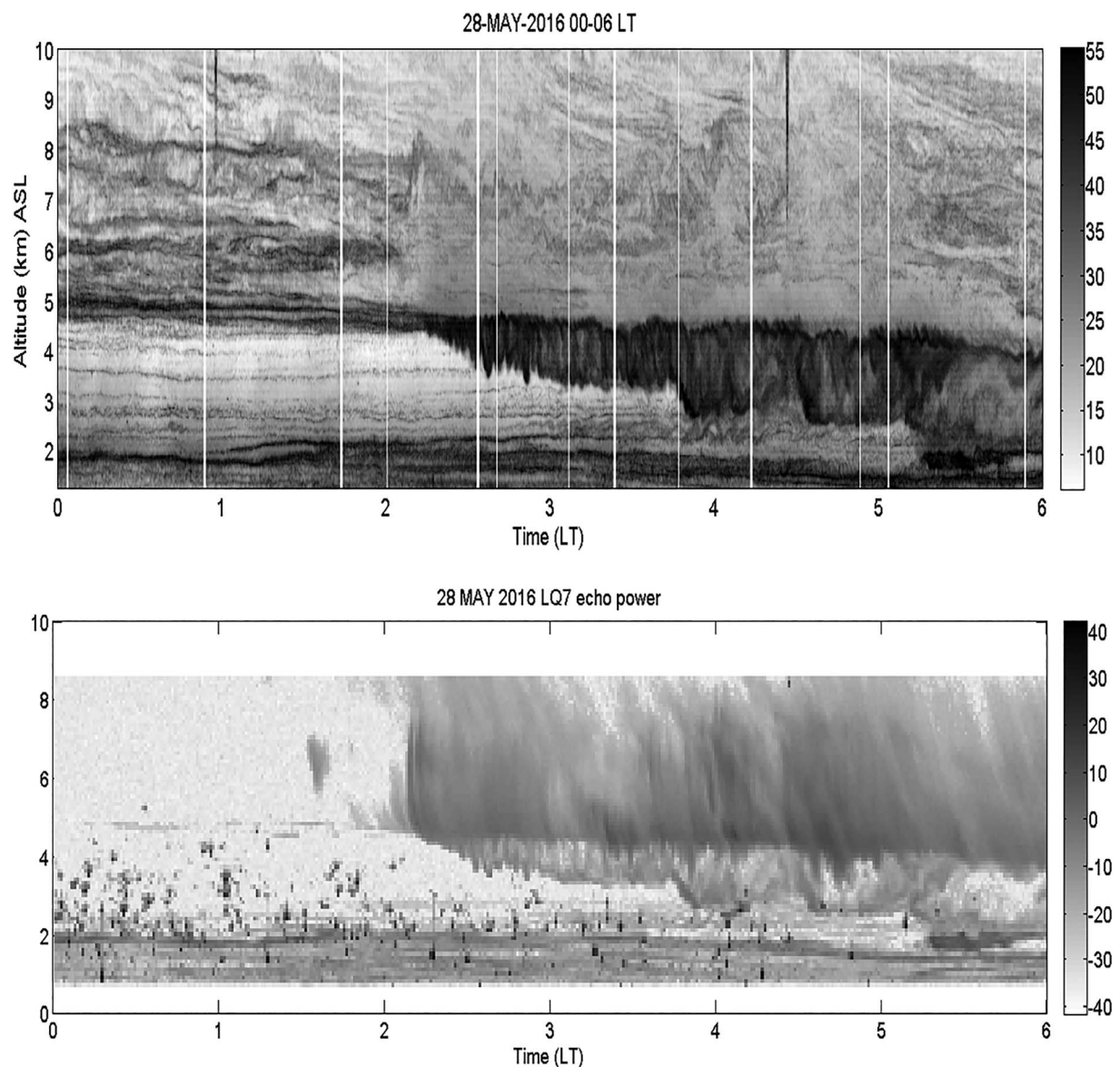


Figure 2. As in Figure 1 but for the midlevel cloud-base turbulence event, which occurred on 28 May 2016. Middle and Upper atmosphere radar and ultrahigh frequency images are shown for the time interval 00:00 to 06:00 LT. ASL = above sea level.

variability, with columnar structures, can be seen in the layer between 15:30 and 18:00 LT. The MCT event lasted over 6 hr, with the layer dissipating at around 24:00 LT. A radiosonde launched at the site sampled it at just the right time around 15:20 LT. Another sampled the conditions at around 13:30 LT, 2 hr before the formation. Their tracks are shown as red lines. UAV flights were also conducted during that day but were confined to lower altitudes. Their tracks appear as black lines.

The lower panel of Figure 1 shows the corresponding image from a 900 MHz LQ7 ultrahigh frequency (UHF) radar deployed at the MU radar site. Since, unlike VHF radars, UHF radar backscatter is affected principally by precipitating particles in the atmosphere and secondarily by turbulence, the image shows essentially the precipitation pattern during the event. The onset of precipitation in the cloud that triggered the MCT below the cloud base can be seen clearly. The MCT structure seen in the two radar images is consistent with each other. This MCT case will be analyzed further.

The second MCT event shown in Figure 2 occurred on 28 May 2016 during the ShUREX 2016 campaign. The MU and UHF radar images are shown between 00:00 and 06:00 LT. A cloudy layer above 5-km

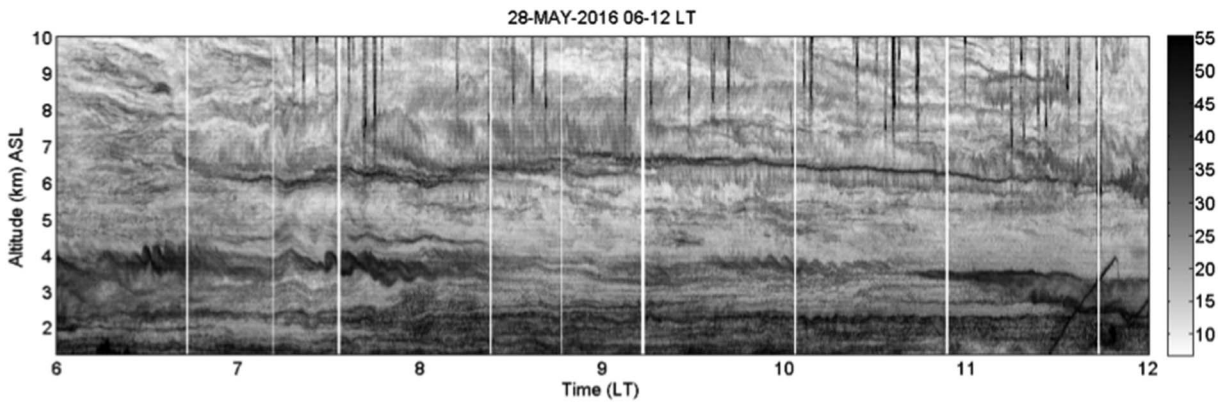


Figure 3. Middle and Upper atmosphere radar image for the weaker midlevel cloud-base turbulence event, which followed the one shown in Figure 2 on 28 May 2016. ASL = above sea level.

altitude, with two thin sheet-like structures with a layer sandwiched between them at its bottom, and a much drier air immediately below can be seen clearly in the MU radar image from 00:00 to 02:15 LT. At around 02:15 LT, precipitation starts to occur in the cloudy layer and the initiation of the MCT layer immediately below the cloud base can be seen. The MCT layer grew slowly to 1,450 m in 90 min starting at 02:20 LT, then grew quickly to 2,000-m thickness at around 03:40 LT and then remained roughly the same before growing further at around 05:20 LT and dissipating. The cloud base descended from 5 km AGL to about 4 km during that time. The UHF radar image in Figure 2 (bottom panel) confirms the onset of precipitation around 02:10 LT. No UAV flights or radiosonde launches were made during this MCT event.

A weaker MCT event followed the strong event on 28 May 2016, starting around 10:45 LT below the cloud base at 3.5-km altitude (Figure 3). The MCT layer grew to 700 m in thickness by 12:30 LT. The UAV Flight 08 sampled this event. Weak Kelvin-Helmholtz instability events can also be seen to occur at the cloud base prior to the MCT event at around 06:30, 07:30, and 10:00 LT, indicating the presence of wind shear at the cloud base during those times.

Figure 4 shows the MCT event on 5 June 2015. It started at about 08:20 LT, and the layer grew very rapidly to 900 m in thickness and then slowly to 2,500-m thickness with the cloud base descending from 5 to 4 km. As can be seen from both images, a UAV penetrated the MCT layer but crashed into the forest after a fast uncontrollable descent shortly thereafter.

Figure 5 shows the MCT event that occurred on 11 June 2015 between 06:20 and approximately 10:00 LT, with the layer growing rapidly to 1,375-m thickness in about 1.25 hr. The cloud base descended from 5.5 km to around 3 km by the time the MCT dissipated. A UAV managed to sample this event in its final decaying stages. Interestingly, the UHF radar image shows precipitation only in the cloudy layer up to around 09:00, at which time it penetrates below the cloud base. That is the time when the MCT event starts to weaken significantly. Prior to 09:00, the precipitated ice/snow particles evaporated rapidly in the MCT layer and so do not show up in the UHF radar image. A dark band indicating the 0 °C isotherm can also be seen in the UHF radar image at an altitude of 5 km starting around 9:00 LT.

Figure 6 shows a weak MCT event on 4 June 2016, which developed around 08:20 LT and lasted till around 11:00 LT. Figure 7 shows this event dissipating around 12:00 LT, but a fresh MCT layer develops around 12:50 LT and extends to about 1,500-m thickness by 14:00 LT. Thus, the layer grew in thickness by 1,500 m in 70 min. The MCT layer was sampled by a UAV between 16:30 and 17:30 LT, but the layer had weakened significantly by that time. K-H billows can be seen inside the cloud at around 14:30 LT.

MCT events were also observed at higher altitudes of 6 to 9 km, but these events were generally, but not always, weaker than the ones seen at lower altitudes. Figure 8 shows such a high-altitude event on 8 June 2016.

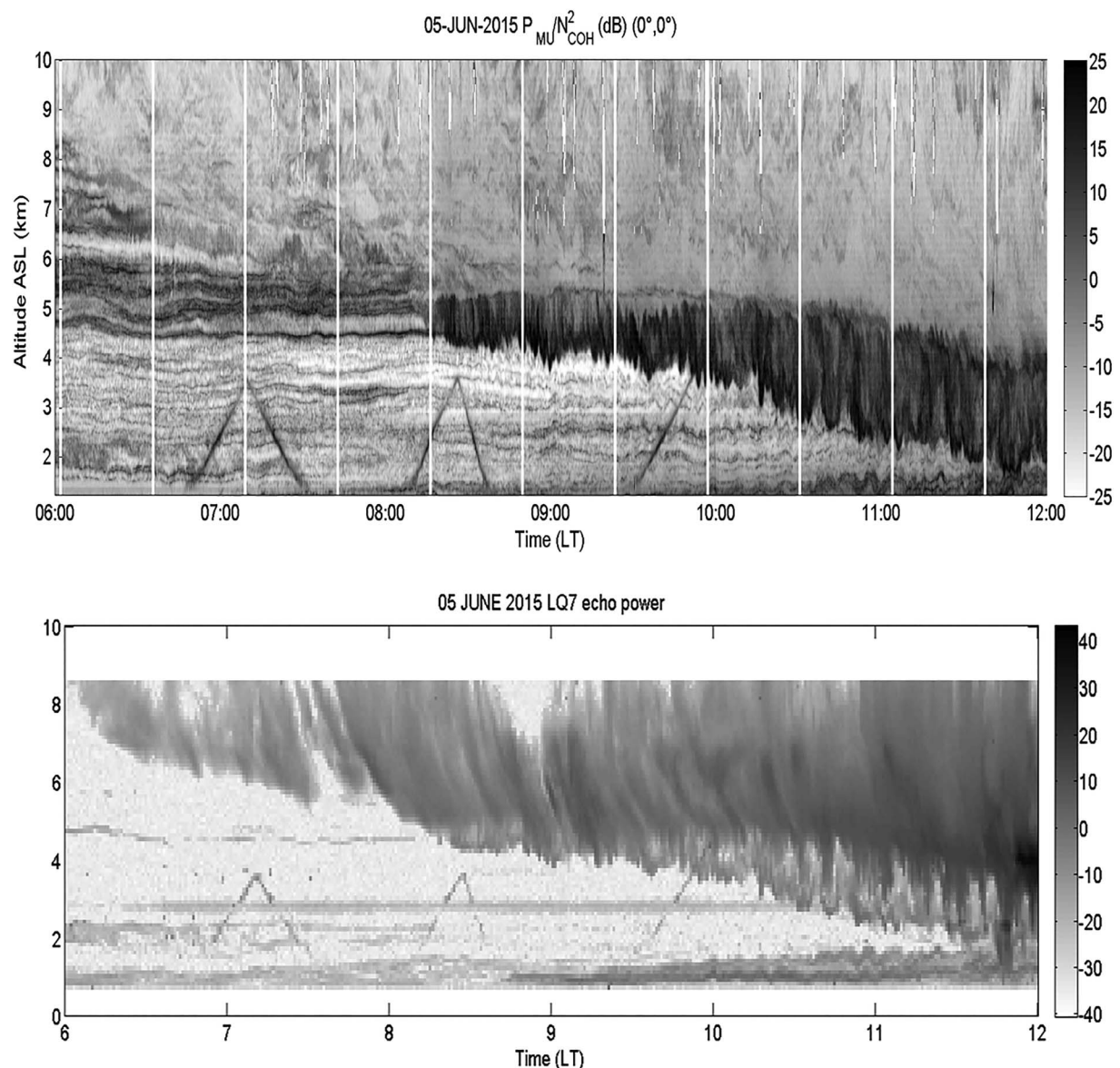


Figure 4. As in Figure 1 but for the midlevel cloud-base turbulence event, which occurred on 5 June 2015. Middle and Upper atmosphere radar and ultrahigh frequency radar images are shown for the time interval 06:00 to 12:00 LT. ASL = above sea level.

Table 1 summarizes the MCT events observed by the MU radar during the two campaigns (overall duration of 36 days), where asterisks denote the events discussed above. To summarize, atmospheric conditions during which a moist air mass is advected over a dry layer are quite common during rainy seasons and such conditions are conducive to MCT. MCT events were quite common at the MU radar site during ShUREX 2015 and 2016 campaigns. However, their onset was not known in advance to plan launches of radiosondes and UAVs to sample the events. UAV flights were restricted by aviation authorities to daytime conditions and altitudes less than 4 km, preventing sampling MCTs that occurred during the night and during the day but above 4-km altitude. Whatever sampling we did was purely by chance. However, the situation has changed. Probability of occurrence of MCT can be predicted well in advance and Japan Meteorological Agency (JMA) has started to issue MCT forecasts for use by air traffic authorities. The 6-hr forecasts appear to be reasonably accurate for planning UAV and radiosonde launches. During the ShUREX 2017 campaign, JMA forecasts of potential MCT occurrence were almost always confirmed later by the MU radar. However, because of the anomalous weather conditions in the summer of 2017, MCT events, especially at low

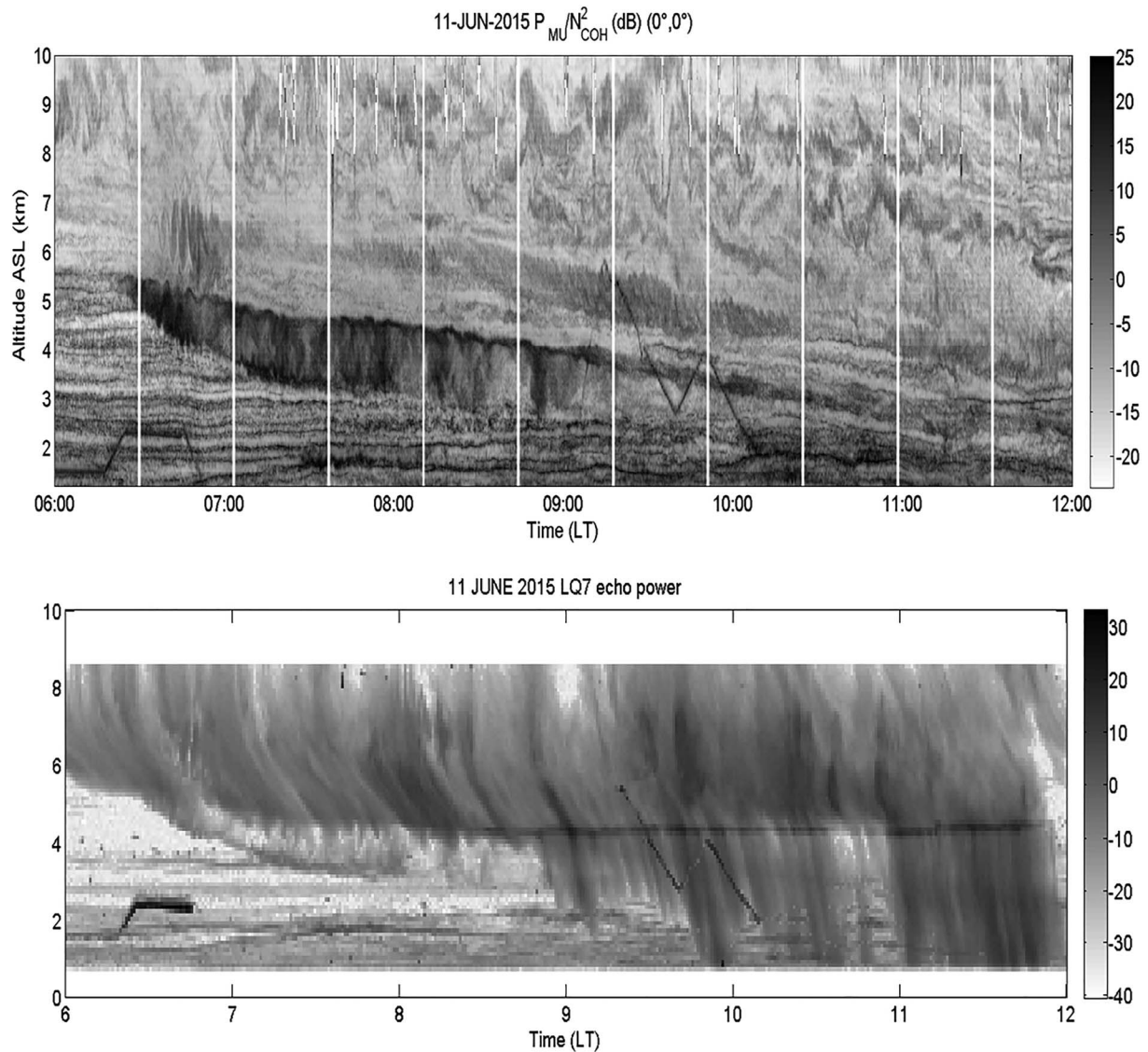


Figure 5. As in Figure 1 but for the midlevel cloud-base turbulence event, which occurred on 11 June 2015. Middle and Upper atmosphere radar and ultrahigh frequency radar images are shown for the time interval 06:00 to 12:00 LT. Spectacular Kelvin-Helmholtz billows can also be seen within the cloud immediately above its base from approximately 06:30 to 06:50 LT. ASL = above sea level.

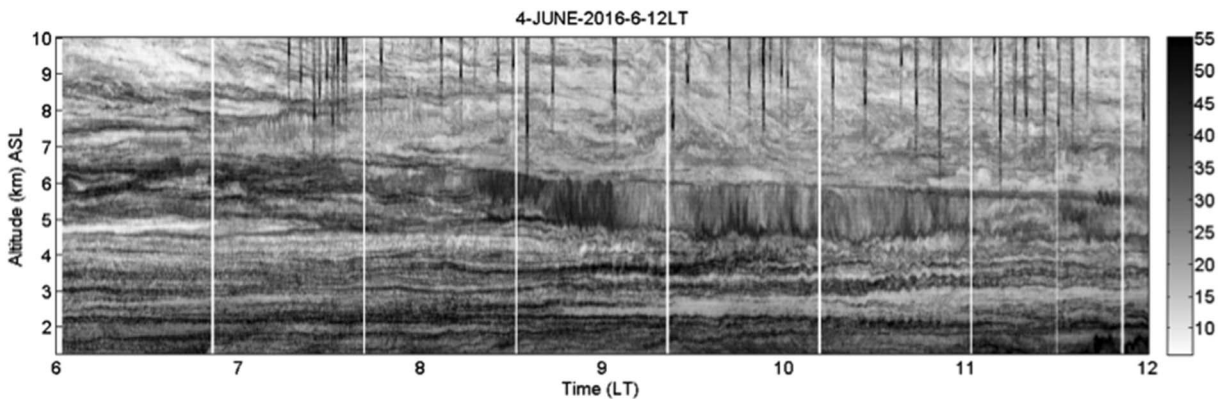


Figure 6. Middle and Upper atmosphere radar image on 4 June 2016 showing a weak midlevel cloud-base turbulence event. ASL = above sea level.

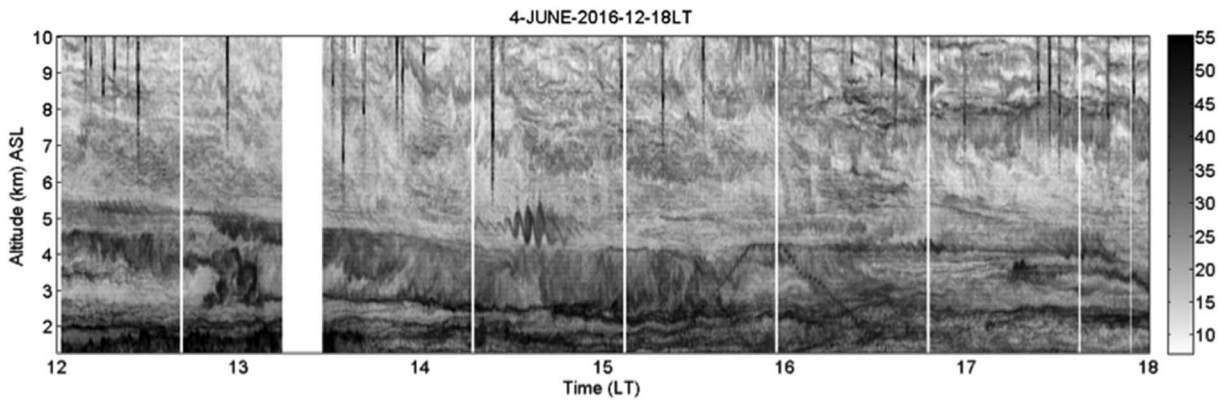


Figure 7. Middle and Upper atmosphere radar image on 4 June 2016 from 12:00 to 18:00 LT, showing a fresh midlevel cloud-base turbulence event develop at 12:50 LT. Kelvin-Helmholtz billows can be seen inside the cloud around 14:30 LT. ASL = above sea level.

altitudes amenable to probing by UAVs, were scarce. Such JMA forecasts should be helpful in future ShUREX campaigns.

Finally, it is important to recall that MCT refers to turbulence *below* the cloud base generated by sublimation of ice/snow particles falling out of the cloud into the dry air below. Both MU and UHF radar images (e.g., Figure 2) clearly delineate the cloud base above the MCT region. In MU radar images, the cloud with ongoing precipitation shows up as a chaotic region and when present, MCT manifests as a much darker region with vertical striations due to convective plume activity. Cloud top radiative cooling has long been known (e.g., Lilly & Schubert, 1979) to be capable of producing turbulence *inside* the clouds near their upper portions, which may or may not result in entrainment at the cloud base. Chen and Cotton (1983) also state “Cloud top cooling occurs principally within the upper part of the mixed layer.” Thus, we can rule out cloud top radiative cooling as the cause of MCT. Also, we have seen no evidence of orographic wave activity during MCT phenomena and MU radar observations often show MCT occurring at altitudes as high as 7 to 9 km without any wave activity. Studies by Kudo (2013) and Kudo et al. (2015) also confirm that MCT is caused by convective instability.

2.2. A Simple Analytical Model

While Kudo (2013) attributed MCT to Rayleigh-Taylor instability, MU radar observations clearly show well-developed convective turbulence in the MCT very much similar to that in a CBL. Since MCT is triggered in most cases by ice/snow precipitation falling below the cloud base (typical temperature ~ 261 K) into a dry air layer below and sublimating, question is what sort of precipitation rates are involved and how the

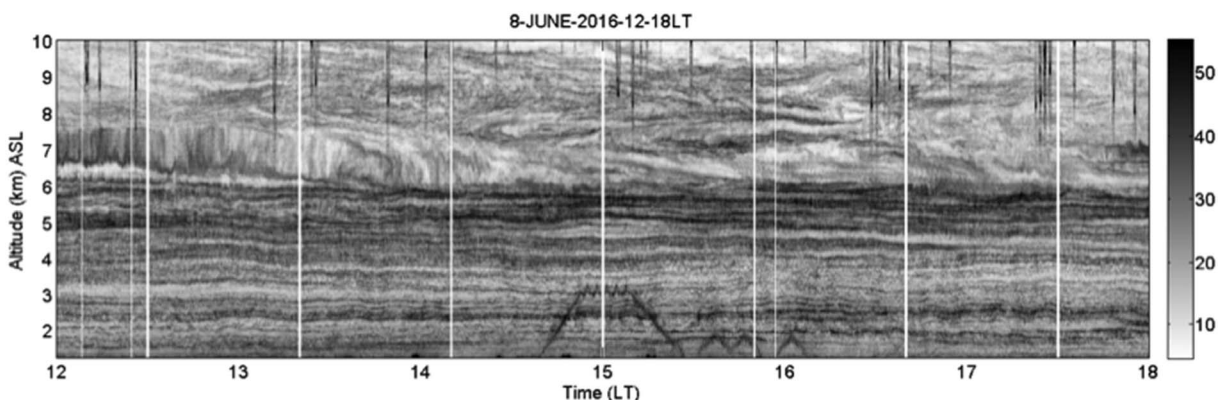


Figure 8. Middle and Upper atmosphere radar image on 8 June 2016, showing an midlevel cloud-base turbulence layer at a higher altitude between 6 and 7.5 km. ASL = above sea level.

Table 1
MCT Events Observed During ShUREX 2015 and 2016 Campaigns (Asterisks Denote the Cases Discussed in the Text; Durations Rounded off to Nearest 15 min)

Date	Duration	Top (LT)	Depth (km)	Subsidence (km)	Comments
2 June 2015	05:30 to 07:30	~7.5	~2		
* 5 June 2015	08:15 to 12:15	5.5 to 4.0	1 to 2	1.5	Strong
5 June 2015	12:15 to 20:00	~4.5	< 0.5		MLT?
7 June 2015	13:00 to 19:30	7.0 to 6.5	0.5 to 1	1.0	
8 June 2015	MU radar turned off				
9 June 2015	11:00 to 19:50	5.5 to 6.5	1 to 2	-1.0	
10 June 2015	03:15 to 05:30	~8.0	0 to 1.5		Weak
11 June 2015	00:45 to 02:30	7.5 to 7.0	0.5 to 0.7	0.5	Weak
* 11 June 2015	06:30 to 09:00	5.5 to 4.0	0 to 1.5	1.5	Strong
11 June 2015	09:00 to 10:15	4.0 to 3.5	1.5 to 1.0	0.5	Weak follow-on
* 13 June 2015	15:00 to 00:00	6.0 to 4.5	0 to 1.5	1.0	Lasted long
25 May 2016	16:30 to 22:00	8.0 to 10	0.5 to 1.5		MLT?
* 28 May 2016	02:15 to 06:00	5.0 to 4.5	0 to 1.8	0.5	Strong
* 28 May 2016	10:45 to 12:15	~3.5	0 to 1		Weak
* 4 June 2016	08:15 to 11:00	7 to 6.5	1 to 1.2	0.5	
* 4 June 2016	12:45 to 16:50	5.5 to 5	0 to 1.5	0.5	Weak
* 8 June 2016	09:45 to 14:00	8.5 to 8	~1	0.5	Weak
11 June 2016	08:45 to 13:00	9 to 7.5	0 to 1.2	2.5	Weak
12 June 2016	05:15 to 08:30	~8.5	0 to 1		Weak

Note. MCT = midlevel cloud-base turbulence; ShUREX = Shigaraki UAV Radar Experiment; MU = Middle and Upper atmosphere; MLT = melting layer turbulence.

precipitation rate is related to the turbulence parameters. We explore these issues with a simple analytical model to establish approximate levels of TKE and its dissipation rate.

Convection initiated by heating of the ground after sunrise is a well-explored problem (see references cited in section 1). For a stably stratified atmosphere with an initially linear stratification, it can be shown that if there is no entrainment at the top of the CBL (the so-called nonpenetrative convection), the CBL depth D increases with time t as

$$D \sim t^{1/2} \quad (1)$$

as shown by classical laboratory experiments by Deardorff et al. (1969, 1980) and Willis and Deardorff (1974). This changes somewhat when the entrainment is taken into account. Both Willis and Deardorff (1974) and Kantha (1980) showed that the buoyancy flux Q_e at the top of the CBL, where turbulent entrainment brings in air above into the CBL, follows the simple relationship:

$$\frac{Q_e}{Q_0} = 0.2 \quad (2)$$

for the parameter range of interest in the atmosphere, where Q_0 is the buoyancy flux at the bottom of the CBL.

The velocity scale in a CBL is the Deardorff velocity scale (Deardorff, 1970; Kantha & Clayson 2000):

$$w_* = (Q_0 d)^{1/3} \quad (3)$$

where d is the CBL depth. Turbulence parameters inside the CBL scale with w_* . For example, the turbulence velocity

$$q = c w_* \quad (4)$$

where c is a constant with a value of around one, so that

$$\text{TKE} = \frac{c^2 w_*^2}{2} \quad (5)$$

The different components of turbulence velocity are approximately

$$\overline{u^2}, \overline{v^2} \sim 0.25q^2, \overline{w^2} \sim 0.5q^2 \quad (6)$$

Also, the TKE dissipation rate inside the CBL is given by

$$\varepsilon \simeq 0.4Q_0 \quad (7)$$

There are two limits possible. One is the trivial limit, when the precipitation exiting the cloud base does not evaporate and hence does not trigger MCT. The other limit is one where the precipitation exiting the cloud base is immediately sublimated (or evaporated). The reality is somewhere in-between. If we assume the latter limit, then MCT is very much analogous to the conventional CBL, but driven by the destabilizing buoyancy flux at the top of the MCT (i.e., immediately below the cloud base). The resulting heat flux (W/m^2) is

$$F_0 = \rho_w L \left(\frac{\dot{r}}{3,600 \times 1,000} \right) \quad (8)$$

where \dot{r} is the precipitation rate (mm/hr), $L = 2.835 \text{ MJ/kg}$ (2.5008 MJ/kg) is the latent heat of sublimation (evaporation) at 0°C , $\rho_w = 1,000 \text{ kg/m}^3$ is the density of water. The heat flux amounts to about 788 (627) W/m^2 for a precipitation rate of 1 mm/hr . This is substantial. The buoyancy flux is then

$$Q = \frac{g}{\Theta} \left(\frac{F_0}{\rho_a c_{pa}} \right) \quad (9)$$

where $\rho_a \sim 1.0 \text{ kg/m}^3$ is the density of air at the altitude of the MCT, $c_{pa} = 1006 \text{ J}\cdot\text{kg}^{-1}\cdot\text{K}^{-1}$ is the specific heat of air, and Θ is the potential temperature taken as $\sim 300 \text{ K}$. With these values, $Q \sim 0.025$ (0.02) m^2/s^3 for sublimation (evaporation) at a precipitation rate of 1 mm/hr .

The most important quantity in the MCT process is the precipitation rate immediately below the cloud base, which has never been measured, although rough estimates could be made using an operational or research type atmospheric model (e.g., Weather Research and Forecast, WRF). We also do not know its variability in time, which is crucial to the evolution of MCT layer with time. Just as the temporal evolution of the CBL depends on the solar radiation reaching the ground, the evolution of the MCT depends on the precipitation rate immediately below the cloud base. However, measurements are difficult at best and nonexistent at present. But we can show what rates are compatible with existing turbulence measurements in the MCT. Assuming $c = 1$, for a TKE value of say $3.67 \text{ m}^2/\text{s}^2$, $w_* \sim 2.7 \text{ m/s}$ (and the root mean square vertical velocity $\rho_w \sim 1.9 \text{ m/s}$). For a MCT layer depth of, say, $1,000 \text{ m}$, we have $Q \sim 0.02 \text{ m}^2/\text{s}^3$, which implies a precipitation rate of roughly 0.8 mm/hr .

The dissipation rate $\varepsilon \simeq 0.4Q \sim 0.008 \text{ m}^2/\text{s}^3$ and eddy dissipation rate widely used in aviation studies, equal to $\varepsilon^{1/3}$ is $0.2 \text{ m}^{2/3}/\text{s}$, indicating moderate level turbulence. This is similar to the levels measured inside MCTs by the radar during ShUREX campaigns. Note that $\frac{F_0}{\rho_a c_{pa}} \sim 0.61 \text{ Km/s}$.

Furthermore, using the expression for the dissipation rate (e.g., Kantha, 2003; Kantha & Carniel, 2009; Kantha & Clayson, 1994, 2004),

$$\varepsilon = \frac{q^3}{B_1 \ell} \quad (10)$$

where $B_1 \sim 16.6$ and ℓ is the turbulence macroscale, we can estimate the turbulence macroscale within the MCT. Using equations (3), (7), and (10), it is easy to show that $\ell \sim 0.15c^3 D$, so that the turbulence macroscale is about 105 m , for $c = 1$. The simple model presented above can be used to estimate the precipitation rate of ice/snow particles from radar measurements of σ_w .

It is interesting to note that occasionally, turbulent layers somewhat similar in appearance to MCT layers, but with much weaker backscatter intensity levels were observed (but not as frequently) in backscatter images of the MU radar (not shown) operated in range imaging mode. The corresponding UHF radar

image displayed a dark band corresponding to 0 °C isotherm (an example can be seen in the lower panel of Figure 5) at the top edge of the layer. It is quite possible that the generation mechanism of such layers is similar to MCT, but with conditions conducive only to melting of the precipitated ice/snow particles and not sublimation. In that case, L in equation (8) represents the latent heat of fusion of water (~ 0.337 MJ/kg), so that for the same precipitation rate \dot{r} , the buoyancy flux is 11.7% of that corresponding to a MCT. So for the same layer depth then, w_* is about 49%, TKE is 24%, and ϵ is 11.7% of an equivalent MCT. This may be the reason for weaker backscatter from such layers as seen by the MU radar. Note that the presence of 0 °C isotherm in UHF radar images is suggestive, but not a guarantee of occurrence of melting layer turbulence (MLT), which happens when the ice particles melt instead of sublimating (a good example is Figure 5). The latent heat released by melting is much smaller than in a MCT and as such, it must be large enough to trigger convective instability in the layer below the cloud base, which must also be dry enough. The preconditions for convective instability are almost always satisfied for an MCT, but not an MLT. This might be one reason that 0 °C isotherm is seen in UHF in Figure 5, but MU radar does not indicate the presence of a MLT layer.

The initial increase in MCT thickness can be approximated as proportional to $t^{1/2}$, since for nonpenetrative convection for linear stratification:

$$D = \left(\frac{F_0}{\rho_a c_{pa} \frac{d\theta}{dz}} \right)^{1/2} t^{1/2} \quad (11)$$

Knowing the lapse rate below the cloud base, the time evolution of MCT depth can be estimated (more accurate estimates can be made for penetrative convection assuming $Q_e = 0.2Q$). For a potential temperature gradient of say 1 °C/km, we get $D \sim 6.6 t^{1/2}$. For the layer to grow to 1,000 m in thickness, the time needed is 6 hr. This is within a factor of 2 of observed values.

More realistically, due to the penetrative nature of convective turbulence (e.g., Deardorff et al., 1969, Kantha, 1980, Stull, 1973), as the layer depth increases, a stable layer forms at the base of the MCT due to entrainment and slows down the growth rate. This may be responsible for the often-observed gradual decrease in the rate of MCT depth increase with time, assuming of course the precipitation rate remains constant. On the other hand, the MCT variability as seen by the radar could also be simply due to the variability in the precipitation rate and/or due to the fact that sublimation decreases the dryness of the layer as time goes on. Other important factors pertinent to the deepening of an MCT layer are the magnitude of static stability, as indicated by the vertical profile of buoyancy frequency in the air column below the cloud base, and the degree of dryness in the dry layer immediately below the cloud base. If the layer below the cloud base has a strong density interface, Turbulence may not be able to erode the interface by entrainment thus limiting the depth of penetration of MCT. Synergistic use of accurate regional weather forecast models (to estimate the precipitation rate at the cloud base) and Stratosphere-Troposphere radars such as the MU radar to monitor MCT structures (and the turbulence levels within) would be helpful in better understanding of the MCT phenomena in the atmosphere. Use of UAVs and sondes to probe the MCT structure in near-real time guided by the radar images would also be quite useful.

The analogy of a CBL used in the simple model of MCT described above requires the assumption of instantaneous sublimation of ice/snow particles immediately below the cloud base. The reality is of course more complicated, but the next level of approximation is to approximate sublimation inside the MCT layer by an exponential decay function, with an assumed e -folding length scale. This is akin to the absorption of blue-green short wave solar insolation in the upper layers of the ocean, which has been modeled successfully using an exponential decay function in turbulent mixing models of the upper ocean (e.g., Kantha & Clayson, 1994, 2004). Such modeling avoids the complication of having to deal with intricate details of solar radiation absorption in oceanic waters. The difference, when applied to sublimation in the dry layer below the cloud base, is that the process cools and moistens the air layer, whereas the penetrative solar radiation heats the upper ocean. Another unfortunate difference is that while the absorption of solar insolation, critical to the state of the upper ocean, has been extensively studied, no such studies of sublimation of ice/snow particles in a dry layer have ever been done, at least to our knowledge. This forces us to assume a reasonable length scale for penetrative sublimation and experiment with its value, pending the

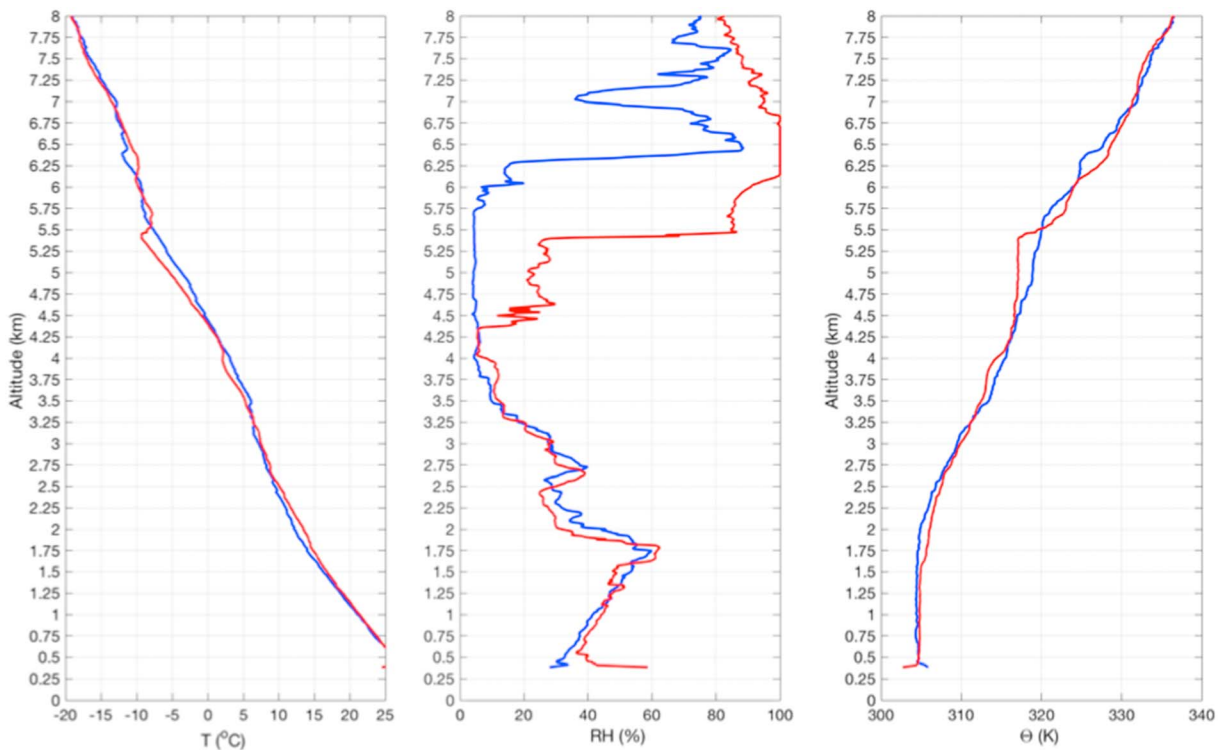


Figure 9. Profiles of temperature, relative humidity (RH), and virtual potential temperature from radiosondes launched from the Middle and Upper atmosphere radar site at 13:00 LT just before (blue) and at 15:25 LT just after (red) the onset of the midlevel cloud-base turbulence. Note the well-mixed middle-level cloud-base turbulence layer in the potential temperature plot spanning the altitude range 4.25 to 5.5 km. The cloud base is at 5.5 km and has descended from 6.25 km.

availability of observational data on the process. We will use this penetrative sublimation model in the one-dimensional second-moment turbulence closure model of mixing in the MCT in section 5. Unlike the simple model detailed in this section, this turbulence model can account for details of stratification below the cloud base, including the presence of any strong, stable density interface, which would inhibit the penetration of MCT below the interface.

3. MCT Event on 13 June 2015

Figure 1 shows this event. It is the only event with (fortuitous) sonde data just before and after the onset of MCT. Figure 9 shows the resulting profiles of temperature, relative humidity (RH) and virtual potential temperature. The well-mixed MCT layer can be seen in the potential temperature plot spanning the altitude range 4.25 to 5.5 km immediately below the cloud base at 5.5 km. The cloud base prior to the onset of precipitation and MCT is at 6.25 km altitude (see Figure 1). The very dry layer immediately below 6.25 km can be seen in the RH profile (blue line). Thus, the data from the sonde just before the onset of MCT confirm the important preconditioning needed for the onset of MCT, namely, the existence of a very dry air layer just below the cloud base needed for sublimation of falling ice/snow particles. See Kudo (2013) for quantitative values of parameters for the onset of MCT.

Figure 10 shows the vertical velocities measured by the vertical beam of the MU radar from 12:00 to 18:00 LT. Up/down drafts exceeding ± 2 m/s can be seen in the MCT layer, as well as the CBL (from 12:00 to 14:40 LT). These are indicative of strong convective motions present in these layers. Figure 11 shows TKE and ϵ , deduced from measured radar spectral width after appropriate corrections for spectral broadening, using the method described in Wilson et al. (2014; see also Kantha et al., 2017 and Luce et al., 2018). High TKE and ϵ levels of similar magnitude can be seen both in the MCT and CBL layers.

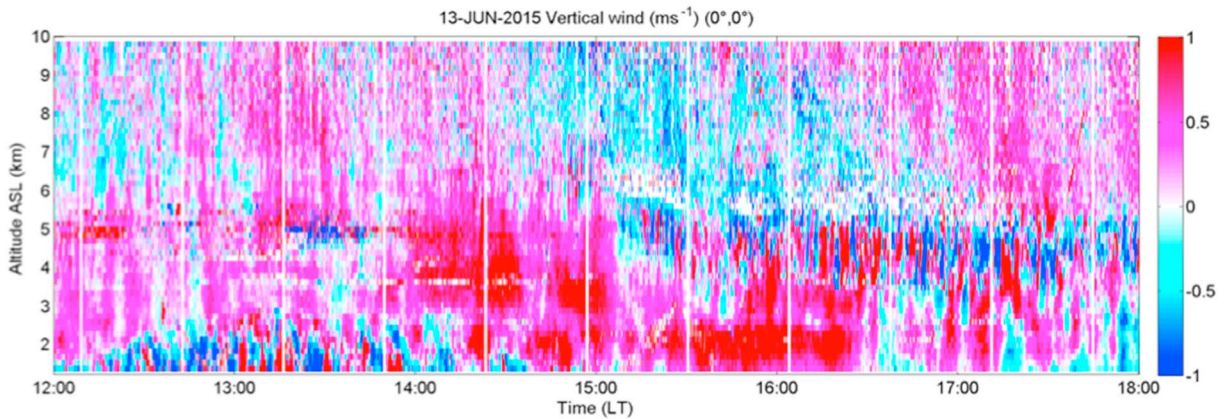


Figure 10. Vertical velocities measured by the vertical beam of the Middle and Upper atmosphere radar. Note the strong up/down drafts exceeding ± 2 m/s in the midlevel cloud-base turbulence layer. ASL = above sea level.

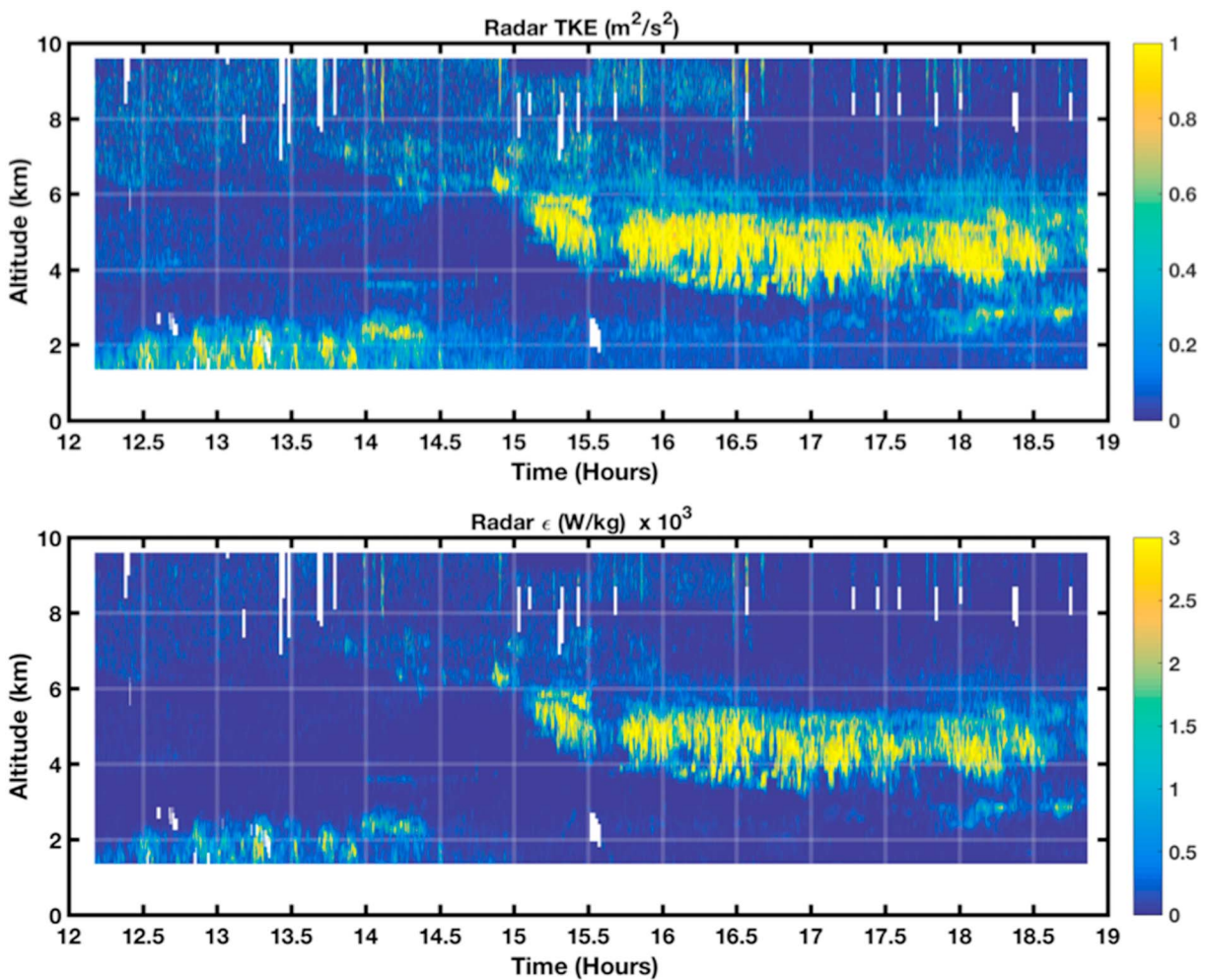


Figure 11. Turbulence kinetic energy (TKE) and ϵ measured by the vertical beam of the Middle and Upper atmosphere radar (and after appropriate corrections applied). Note the high levels of turbulence in both the midlevel cloud-base turbulence and the top of the convective boundary layer. The radar backscatter is available only at altitudes above 1.34 km (above ground level).

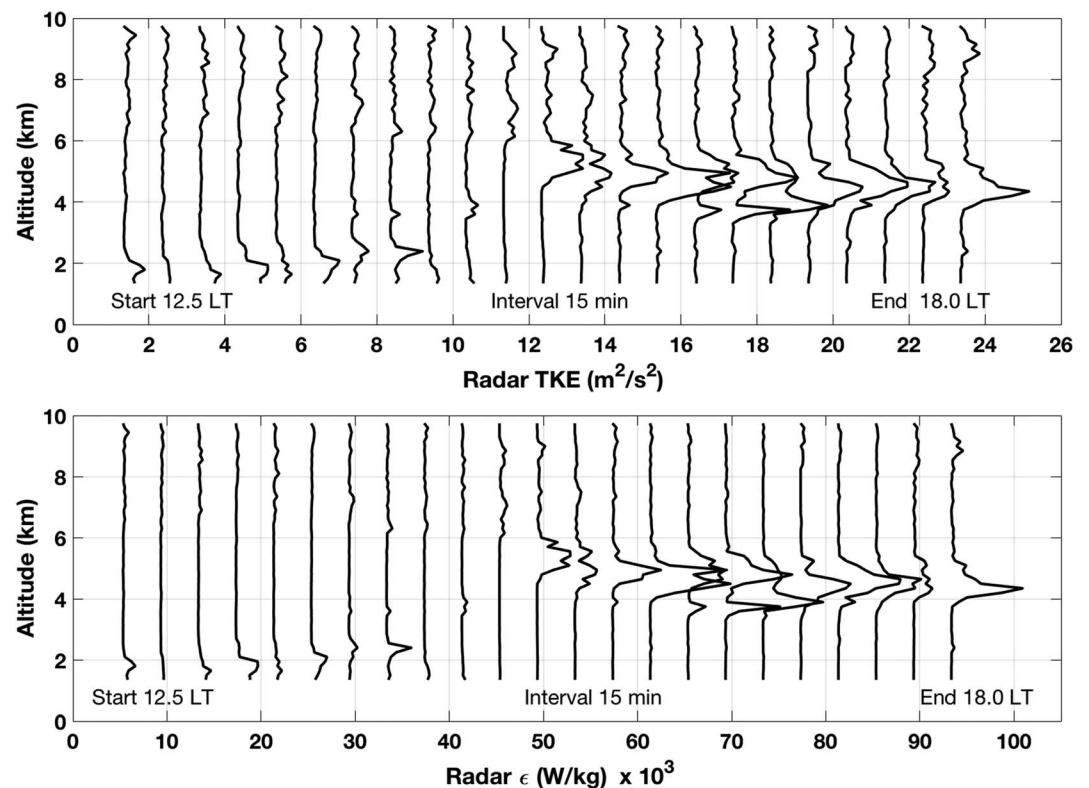


Figure 12. Waterfall plots of 1-min running mean of turbulence kinetic energy (TKE; top panel) and ϵ (bottom panel), starting at 12:30 LT and ending at 18:00, plotted at 15-min intervals. The profiles are offset by 1.0 for TKE and 4.0 for ϵ .

Figure 12 shows a waterfall plot of 1-min running mean of TKE (top panel) and ϵ (bottom panel), plotted at 15-min intervals starting from 12:30 LT and ending at 18:00 LT. CBL top can be seen until 14:30 LT. MCT itself starts between 15:00 and 15:25 LT and lasts till around 18:30 LT (not shown). The subsidence of MCT can also be seen until around 13:30 LT. Largest peak values of TKE and ϵ during the MCT event are roughly $2.0 \text{ m}^2/\text{s}^2$ and $8 \times 10^{-3} \text{ W/kg}$, respectively.

This particular event is conducive to numerical modeling, since conditions before the onset of MCT were available from sonde data for initialization of the 1-D model and radar measurements are available prior to and throughout the MCT event. This is the topic of the next section.

4. One-Dimensional Second-Moment Closure-Based Model of MCT

The first attempts to model the MCT phenomenon were by Kudo (2013) and Kudo et al. (2015). They used radiosonde data collected during the Tanuki 2011 campaign for initialization. However, they used a 3-D local model requiring considerable resources and hence not easily amenable to experimentation. On the other hand, a one-dimensional turbulent mixing model based on second-moment closure of turbulence is well suited to exploring MCT. Lateral advection can be ignored if the conditions conducive to MCT occur over a large enough horizontal scale. Subsidence should, however, be kept in mind, when comparing model results to radar observations, since the cloud base can descend as much as 1 to 3 km during the MCT event.

There has been extensive work on second-moment closure of turbulence over the past several decades, and Mellor and Yamada (1982)-type closure models are now routinely used in 3-D models of both the atmosphere and the global ocean, for both research and operational forecasts. Of these, Kantha and Clayson (1994, 2004, see also Galperin et al., 1988) second-moment closure model is routinely used in ocean models. A typical example is the recent study of mixing in the upper layers of the Arabian Sea (Zhou et al., 2018). One-dimensional and two-dimensional versions have also been applied to the

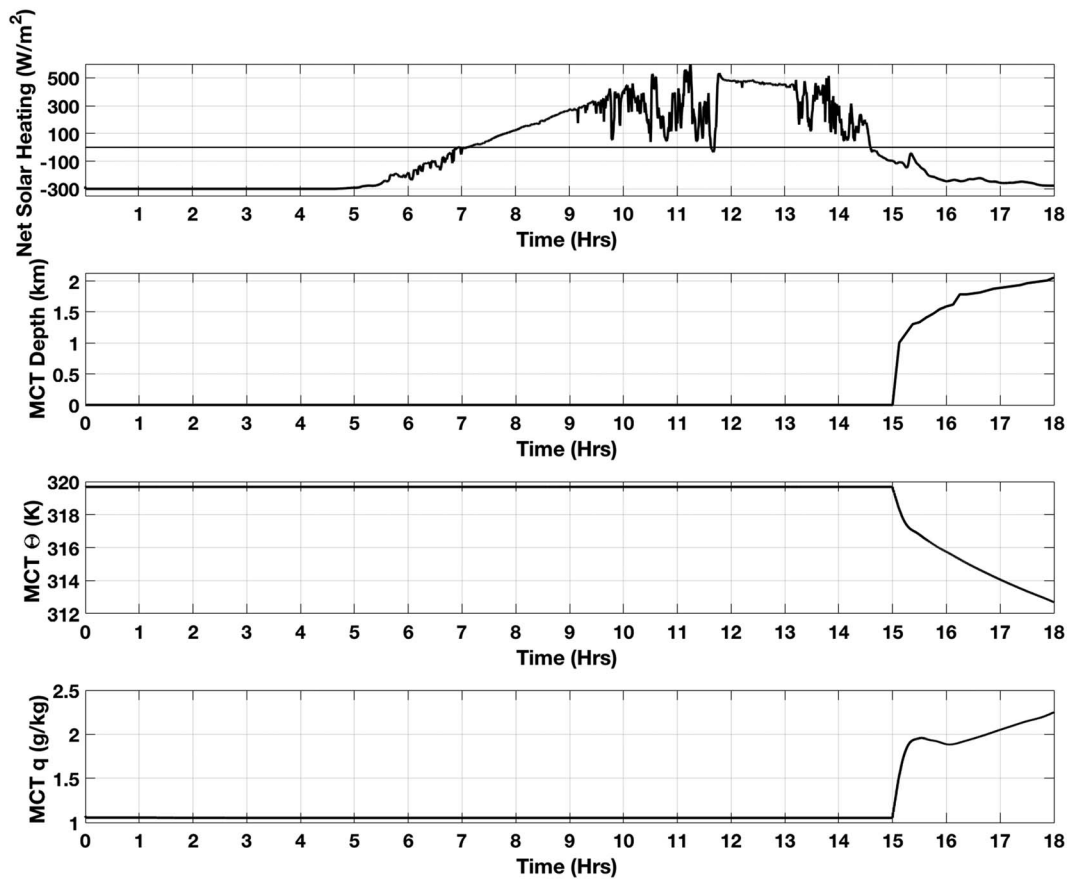


Figure 13. Net solar radiative heating at the ground. MCT = midlevel cloud-base turbulence.

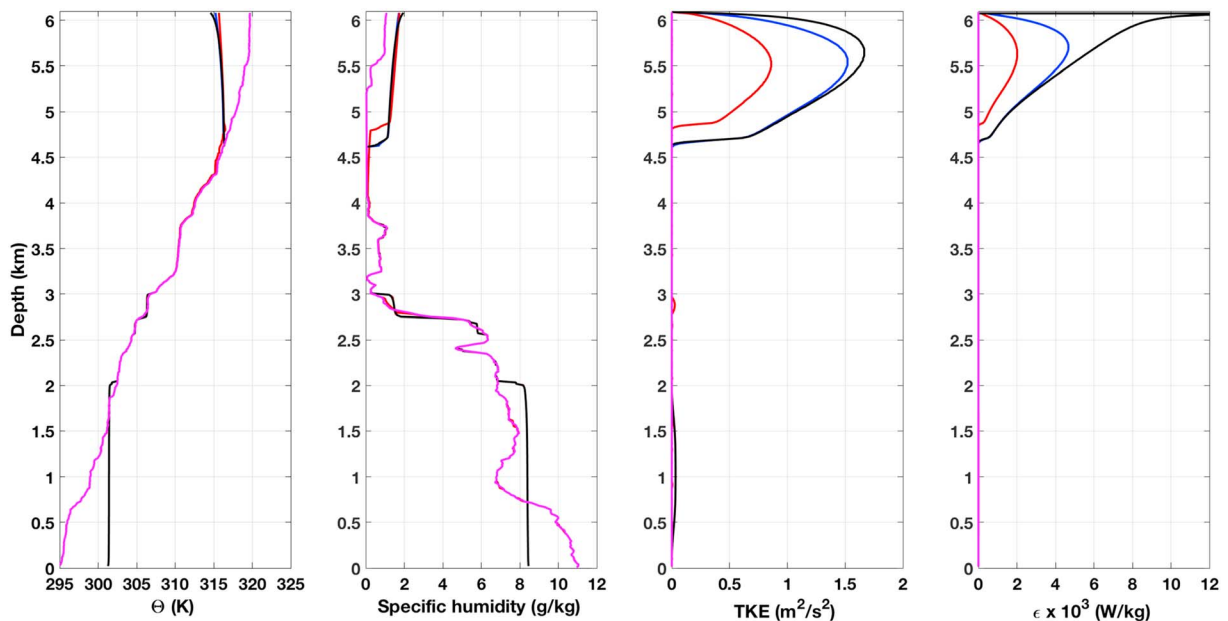


Figure 14. Vertical profiles of potential temperature Θ , specific humidity q , turbulence kinetic energy (TKE), and dissipation rate ϵ of TKE for three values of L_s : 20 m (black), 200 m (blue), and 500 m (red). The precipitation rate is 0.5 mm/hr. See the text for more details.

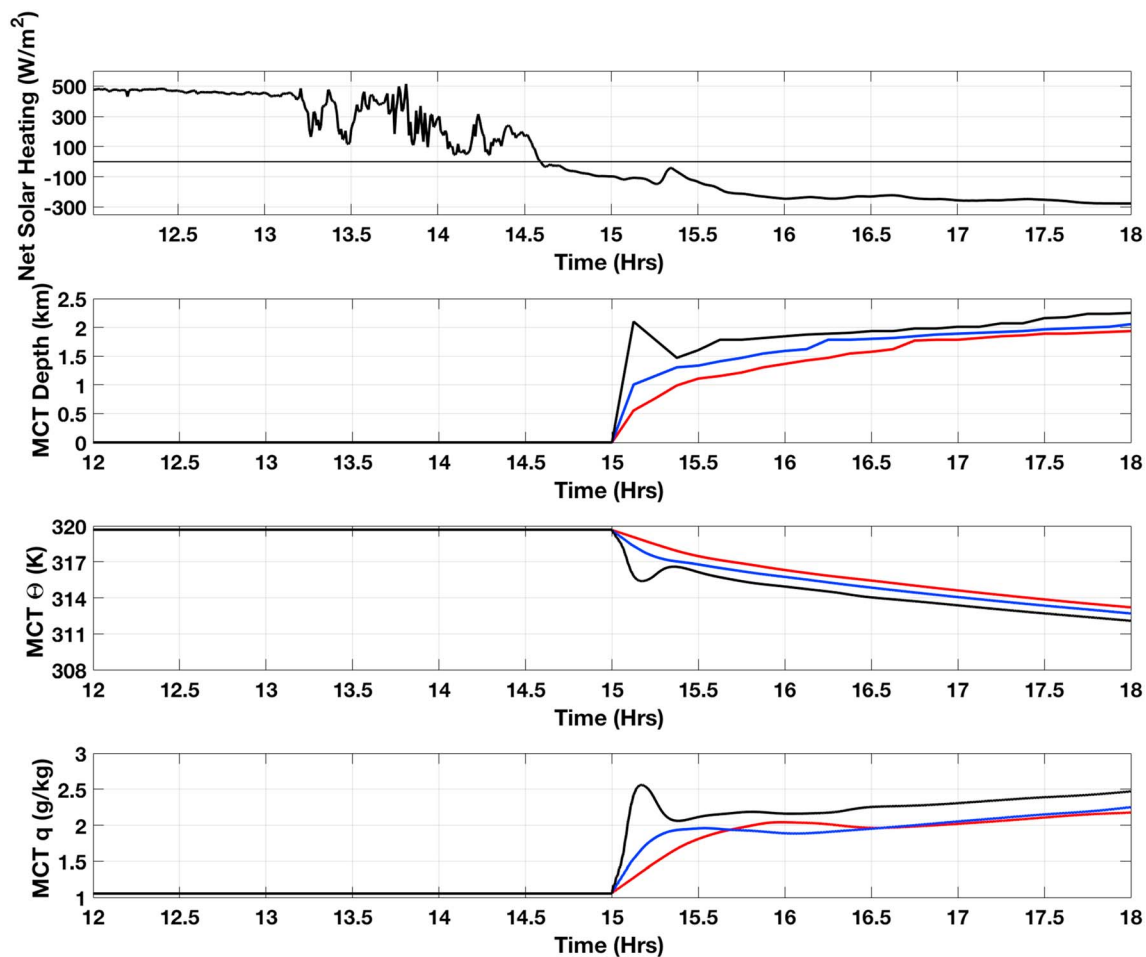


Figure 15. The evolution of the midlevel cloud-base turbulence (MCT) layer for three different values of penetrative sublimation scale L_S : Black = 20 m; blue = 200 m; and red = 500 m. The precipitation rate is held constant at 1 mm/hr.

atmospheric boundary layer (e.g., Kantha & Mellor, 1989, Kantha & Rosati, 1990). The physics of turbulent mixing in the atmospheric boundary layer has also been extensively studied using second-moment closure (e.g., Kantha, 2003; Kantha & Carniel, 2009). In addition to the papers cited above, there are literally hundreds of papers dealing with application of second-moment closure-based turbulence models to mixing in the oceans and the atmosphere.

The Kantha-Clayson model is readily adapted to the atmosphere with appropriate changes in boundary conditions at the top and bottom of the atmospheric column. Here, we have used its 1-D version to model the atmospheric column at the MU radar site during the 13 June 2015 MCT event. The CBL at the bottom of the column is driven by prescribing the net solar heating of the ground (incoming shortwave solar insolation minus the net outgoing longwave radiation). The MCT at the top of the column is driven by prescribed flux of ice/snow particles immediately below the cloud base. The prognostic variables affecting the density of the fluid column are changed from temperature and salinity for the ocean model to potential temperature and mixing ratio for the atmospheric model.

The initial temperature and RH profiles in the modeled atmospheric column were prescribed using data from the sonde launched at 13:00 LT just before the onset of MCT, which shows the dry air layer below the cloud base (Figure 9) needed for the onset of MCT. Solar heating at the bottom was prescribed from measurements at the radar site. Note that the simulation of CBL is not necessary for the simulation of MCT aloft but was included for additional comparison with radar observations.

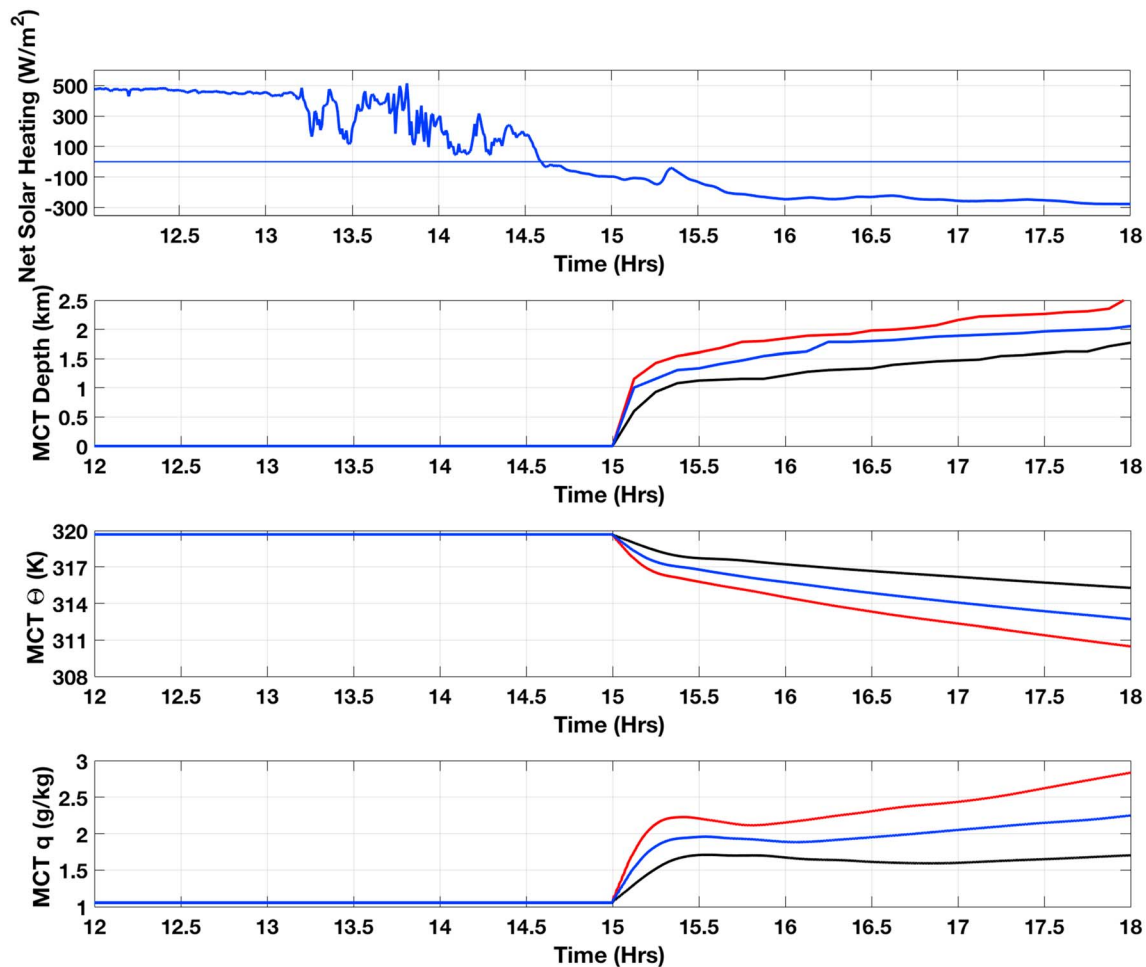


Figure 16. The evolution of the midlevel cloud-base turbulence (MCT) layer for three different values of precipitation rate: Black = 0.5 mm/hr; blue = 1.0 mm/hr; and red = 1.5 mm/hr. L_S is held constant at 200 m.

The main problem in this numerical simulation is the fact that the precipitation rate at the top of the column (i.e., the cloud base) has to be prescribed but is an unknown and unmeasured quantity. Obviously, the magnitude of precipitation and its temporal variability affect the evolution of the MCT. For lack of a better alternative, the precipitation rate was prescribed as 1 mm/hr, the value determined by trial and error to yield approximate agreement with the depth of the MCT at the end of the simulation period. Therefore, this numerical simulation should be regarded as a preliminary attempt, designed to demonstrate the feasibility of modeling MCT with 1-D second-moment closure-based models and not a detailed exploration of the process itself. The latter awaits estimation and/or measurements of precipitation rates during an MCT event and could be the subject of follow-on studies.

The depth of the atmospheric column simulated is taken as 6,090 m. The vertical axis points up, with $z = 0$ denoting the cloud base and $z = -6,090$ m denoting the ground. The vertical resolution of the model is 15 m, and the model time step is 15 s. Simulation starts at 00:00 LT on 13 June 2015. Solar radiation at the ground is prescribed from observations of incoming shortwave solar radiation at the MU radar site, with assumed albedo of 0.25 appropriate to vegetation-covered ground. The net longwave back radiation from the ground is fixed at 300 W/m^2 . Figure 13 shows the net heating rate of the ground in watts per square meter as a function of time. For simplicity, the moisture flux at the ground is put to 0.

The cooling due to penetrative sublimation that drives MCT and the corresponding change in the mixing ratio are determined by

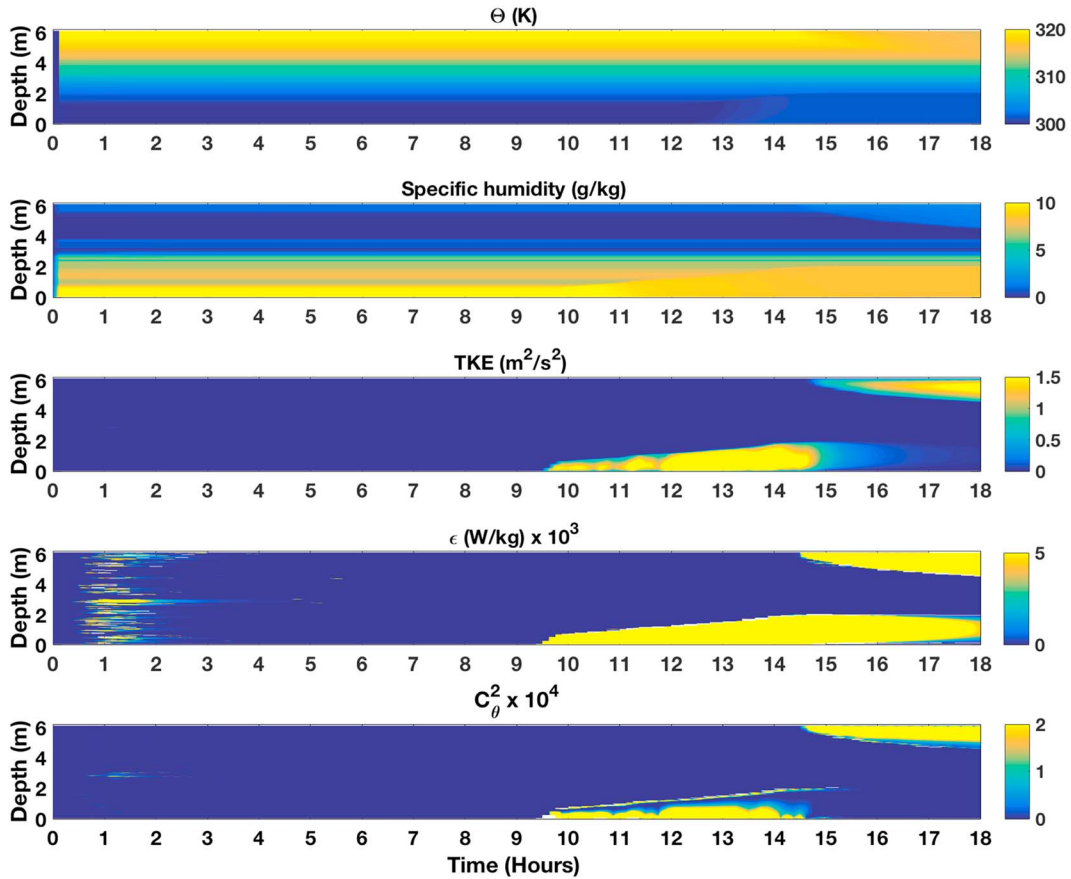


Figure 17. Plot of various properties in the atmospheric column as a function of time. Starting time for the model is 00:00 LT, but 06:00 LT for the plots, since conditions in the modeled atmospheric column do not change until the onset of solar heating of the CBL. Note the evolution of the CBL from approximately 09:30 to 15:00 LT and of midlevel cloud-base turbulence from 15:00 to 18:00 LT. CBL = convective boundary layer; TKE = turbulence kinetic energy.

$$\rho_a c_{pa} \frac{dT}{dt} = -\frac{dQ_h}{dz}; \quad \frac{ds}{dt} = -\left(\frac{1}{\rho_a L}\right) \frac{dQ_h}{dz} \quad (12)$$

where

$$Q_h = Q_{h0} \exp\left(\frac{z}{L_s}\right) \quad (13)$$

and

$$Q_{h0} = \rho_w L \dot{r} \quad (14)$$

T is the temperature, s is the mixing ratio, z is the vertical coordinate with origin at the cloud base, ρ_w is the density of fresh water, ρ_a is the density of air, and L is the latent heat of sublimation. Q_h is the latent heat flux with subscript 0 indicating the value at the cloud base. The \dot{r} is the precipitation rate (m/s).

L_s is the sublimation length scale. The length scale L_s is a complicated function of the dryness of the air, the particle size, among other factors, but for simplicity, is taken as a constant. Various values were explored, and the results for two extreme cases will be presented below. The precipitation rate \dot{r} at the cloud base is taken as 1 mm/hr (corresponding to sublimation cooling rate of 788 W/m²) starting at 15:00 LT (based on MU radar images, see below) and held constant, for lack of a better alternative.

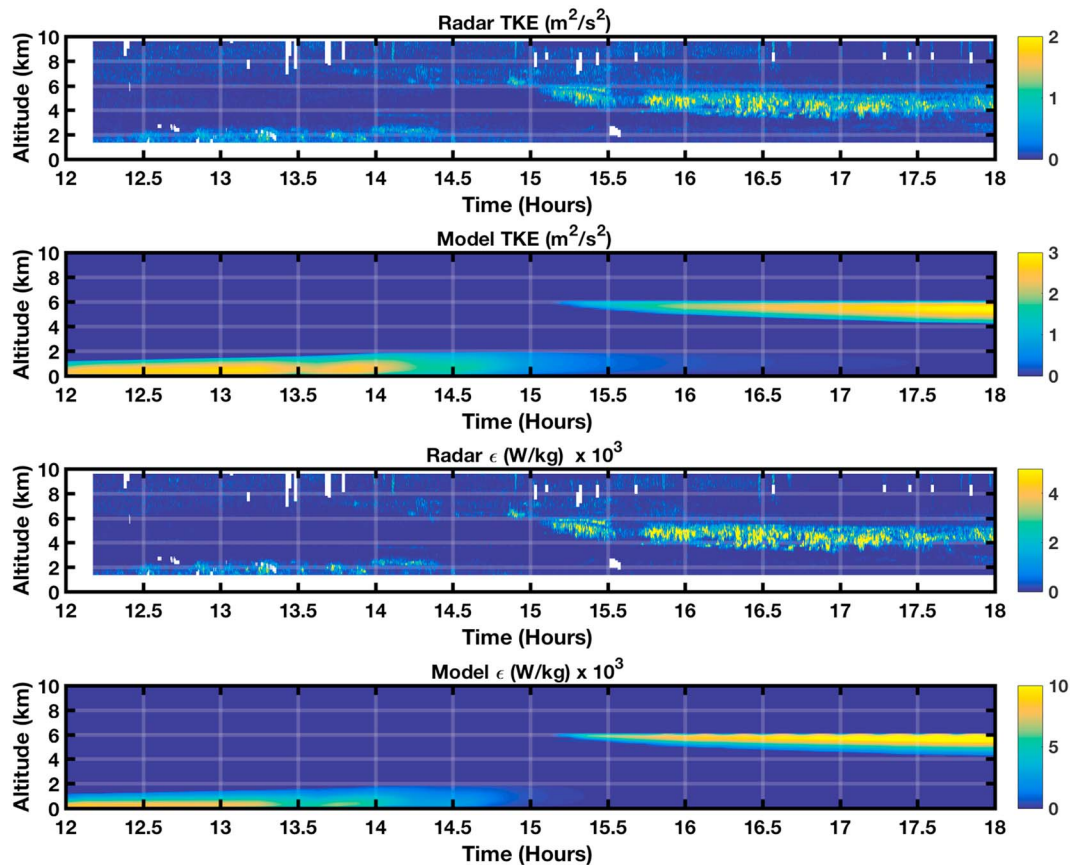


Figure 18. Temporal evolution of the TKE and its dissipation rate from 12:00 to 18:00 LT on 13 June 2015. MCT starts at approximately 15:00 LT, as indicated by the MU radar. Top two panels compare the MU radar-observed TKE values to the modeled values. The bottom two panels compare observed ϵ to modeled values. Note the rough correspondence in magnitudes in both the MCT and convective boundary layer but lack of variability because the precipitation rate is held constant. MCT = midlevel cloud-base turbulence; MU = Middle and Upper atmosphere; TKE = turbulence kinetic energy.

Figure 14 shows the vertical profiles of potential temperature Θ , specific humidity, TKE and dissipation rate ϵ of TKE for three values of L_s : 20, 200, and 500 m at the end of the model simulation, 18:00 LT. Initial profiles at 00:00 LT are shown in magenta. The black lines correspond to $L_s = 20$ m, blue lines to 200 m, and red lines to 500 m. While the value of L_s is important to the magnitude and distribution of TKE and ϵ in the MCT layer, it makes very little difference to Θ and q profiles in the MCT layer. MCT layer deepens rapidly to about 2,000 m at 18:00 LT in all three cases. The maximum value of ϵ in the MCT layer depends on L_s : the lower the value of L_s , the higher the peak value of ϵ . TKE and ϵ values at 18:00 LT are much lower for $L_s = 500$ m than that for $L_s = 20$ m, since in the latter case sublimation in the MCT layer is complete, whereas for the former case, it is not. Therefore, the sublimation length scale has an important effect on the turbulence quantities in the MCT layer, but not as much on potential temperature and specific humidity.

Figure 15 shows the evolution of MCT properties with time for various values of L_s . The black curve corresponds to $L_s = 20$ m, blue curve to 200 m, and red curve to 500 m. While the penetrative sublimation length scale affects the initial phases of MCT layer evolution, the final properties are only slightly altered. This is consistent with the fact that the dominant parameter in the process is the precipitation rate, which is held constant for all three cases.

On the other hand, the precipitation rate is the dominant parameter in the problem. Figure 16 shows the evolution of MCT properties with time for three values of precipitation rate: 0.5 mm/hr (black curve), 1 mm/hr (blue curve), and 1.5 mm/hr (red curve). L_s was held constant at 200 m. Clearly, the precipitation

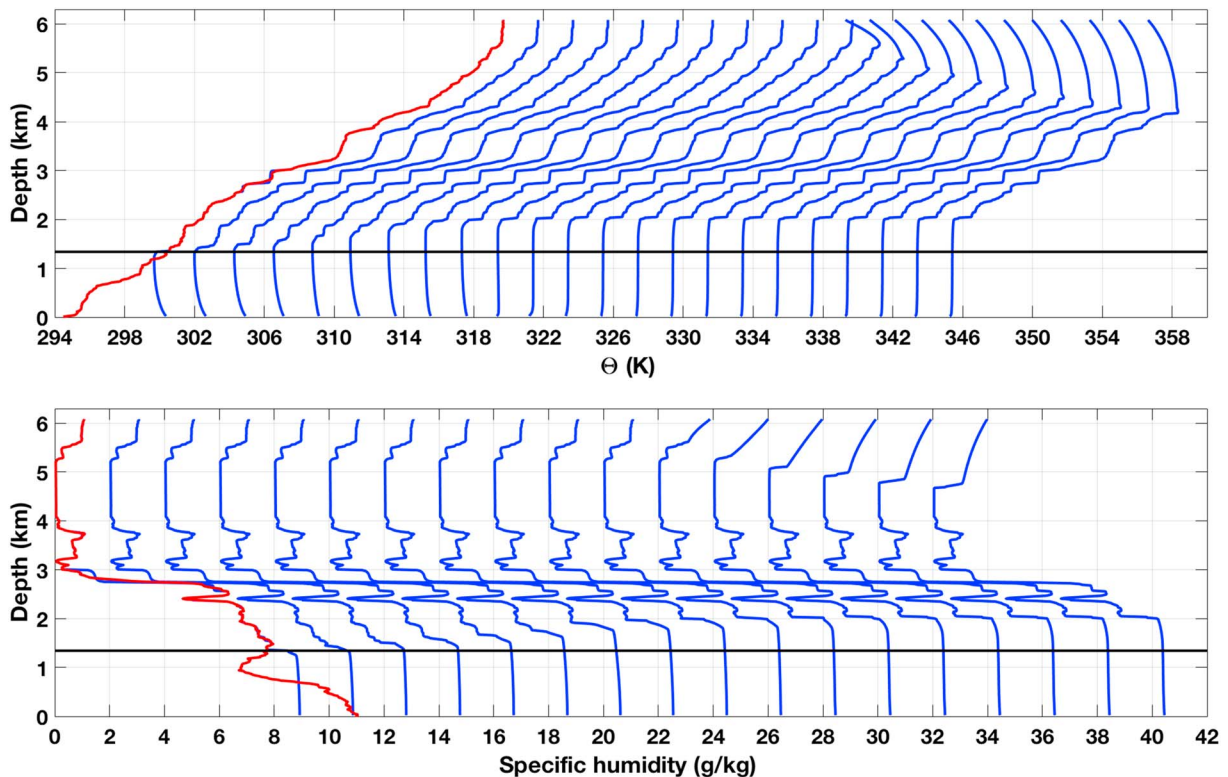


Figure 19. Waterfall plots of potential temperature and specific humidity, starting at 12:30 LT and ending at 18:00, plotted at 15-min intervals. The profiles are offset by 2.0 units for Θ and 2.0 for specific humidity. Initial profile are shown in red.

rate makes a significant difference, with higher rates leading to deeper MCTs, lower MCT potential temperatures and higher specific humidities.

Based on such experimentation, we chose precipitation rate of 1 mm/hr and L_S of 200 m to do a detailed study. Figure 16 shows the evolution of MCT layer for this case (blue curves) starting at 15:00 LT, which quickly grows to about 1.7 km in depth by 18:00 LT. The potential temperature in the MCT layer decreases by about 5 K, and the specific humidity increases by about 0.7 g/kg. Figure 17 shows various properties plotted as a function of time. Note that precipitation of ice/snow particles starts at 15:00 LT. The MCT layer starts evolving at that time. The evolution of the CBL from approximately 09:30 to 15:00 LT and of MCT from 15:00 to 18:00 LT can be seen clearly. Because of the cloud cover, the solar heating on that day was not as strong as it would have been under cloudless conditions.

Figure 18 compares MU radar observed TKE and its dissipation rate to the modeled values. The modeled magnitudes are consistent with observations, but the rich temporal variability seen by the radar is lacking, simply because the precipitation rate is held fixed at 0.5 mm/hr for lack of a better alternative. High levels of turbulence in both the MCT and CBL are evident in the plots. The radar showed that the cloud base was initially at 6-km altitude and it descended to about 5.5 km around 15:30 LT and then stayed at roughly the same altitude till 18:00 LT, end of the model simulation. This descent was not modeled and so the cloud base in the model stays at 6 km.

Overall, the results demonstrate the feasibility of applying a 1-D second-moment closure-based turbulence mixing model to the simulation of the initiation and evolution of an MCT layer. The turbulence physics of the MCT layer is not much different from that of the CBL. Both are driven by destabilizing convective buoyancy fluxes. The only difference is that CBL is heated at the bottom by solar heating, whereas MCT layer is cooled from the top with penetrative sublimation of ice/snow particles dropping below the cloud base. Note that a melting layer can also be simulated by using this model by simply replacing the latent heat of sublimation by latent heat of melting of ice. However, the much smaller

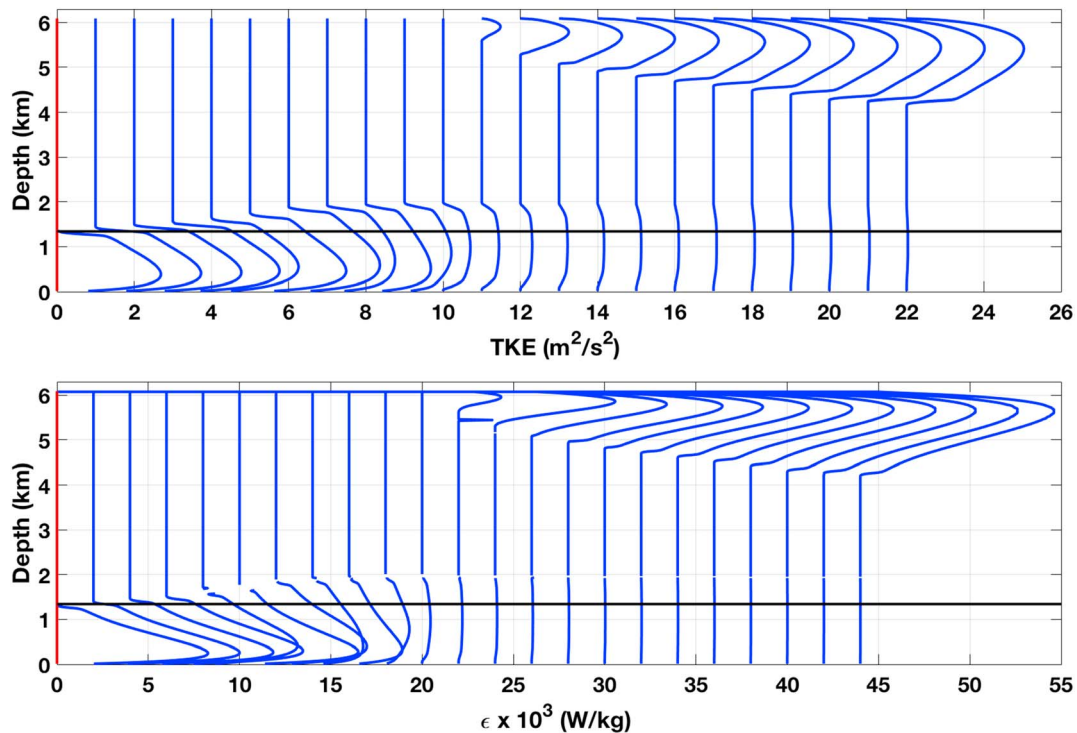


Figure 20. Waterfall plots of potential turbulence kinetic energy (TKE) and ϵ , starting at 12:30 LT and ending at 18:00, plotted at 15-min intervals. The profiles are offset by 1.0 unit for TKE and 2.0 for ϵ . Initial profile are shown in red.

magnitude of the latent heat means that the turbulence levels will be much weaker in a melting layer than in a MCT layer.

While Figures 17 and 18 are helpful in understanding the structure of the MCT layer, an alternative way is to use waterfall plots like Figure 12. Figures 19 and 20 show waterfall plots of Θ , specific humidity, TKE, and ϵ . Figure 20 can be compared directly with Figure 12, showing corresponding radar-derived profiles. There is fair agreement with radar observations, especially given the lack of knowledge of the precipitation rate and its variability in time. The peak TKE values are slightly overestimated, while ϵ values have approximate correspondence. In comparing the two, it is important to remember that the model does not account for the subsidence of the cloud base. Therefore, the top of the MCT layer stays at ~ 6 -km altitude. The model also simulates values down to the ground, whereas radar observations are available only above 1.34 km, indicated by a black line in Figures 19 and 20.

The dominant parameter in MCT evolution is the precipitation rate. The TKE and epsilon values are significantly reduced (enhanced) for precipitation rate of 0.5 (1.5) mm/hr, while the evolution of potential temperature and specific humidity shows similar results to that for the precipitation rate of 1 mm/hr (not shown). In particular, the MCT layer depth at the end of the simulation is roughly the same. This is due to the presence of a strong temperature interface at the depth of about 2 km, which prevents further deepening of the MCT layer. Clearly, the conditions in the air column below the cloud base affect the evolution of the MCT layer.

5. Conclusions

MCT can occur under synoptic conditions, where a moist air mass is advected over a dry one. Around Japan, it occurs typically during the rainy season (Kudo, 2013). In spite of the fact that the first article on MCT was published in 2010 (Luce et al., 2010) and was followed up by Kudo (2013) and Kudo et al. (2015), very little additional work has been done on MCT. We therefore discuss recent observations of MCT at the MU radar observatory in Shigaraki, Japan, during ShUREX 2015 (Kantha et al., 2017) and 2016 campaigns. In addition, we have presented a simple analytical model to estimate approximately the turbulence properties inside an MCT layer. Finally, the MCT event observed by the MU radar on 13 June 2015 has been modeled using a 1-D

second-moment closure-based turbulence model. The intent is to demonstrate the feasibility and utility of such simple numerical simulations of MCT. Clearly, the next steps are a more comprehensive effort to gather relevant data (especially on precipitation rates of ice/snow particles) on MCTs and the application of a comprehensive regional model, such as the WRF model, with appropriate and more comprehensive microphysics of sublimation of ice/snow particles, to more accurately simulate such events. Hopefully, the atmospheric community will be enticed enough by this article to consider more thorough investigations of this fascinating phenomenon through both field observations and comprehensive 3-D regional models. Similarly, while the high-resolution MU radar images gathered during ShUREX campaigns have clearly demonstrated the occurrence of a melting layer (MLT), not much is known at present about this phenomenon. Clearly, more studies would be helpful.

Acknowledgments

L. K. thanks R. Wilson for participation in the ShUREX campaigns organized by L. K. and assisting in collecting the radiosonde data. L. K. and H. L. thank the Japanese Society for Promotion of Science (JSPS) and the Research Institute for Sustainable Humanosphere (RISH) for providing the funding to participate in the campaign. H. L. was funded by CNRS PICS. The hospitality of RISH personnel and director Tsuda to their visitors is exemplary. The MU radar is operated by RISH. Last but not the least, we thank the reviewers for their thoughtful feedback, which improved the paper significantly. The data cited in this paper can be accessed at www.rish.kyoto-u.ac.jp/mu/CaponImages.

References

- Ball, F. K. (1960). Control of inversion height by surface heating. *Quarter Journal of the Royal Meteorological Society*, *86*(370), 483–494. <https://doi.org/10.1002/qj.49708637005>
- Betts, A. K. (1973). Non-precipitating cumulus convection and its parameterization. *Quarter Journal of the Royal Meteorological Society*, *99*(419), 178–196. <https://doi.org/10.1002/qj.49709941915>
- Chen, C., & Cotton, W. R. (1983). A one-dimensional simulation of the stratocumulus-capped mixed layer. *Boundary-Layer Meteorology*, *25*(3), 289–321. <https://doi.org/10.1007/BF00119541>
- Deardorff, J. W. (1980). Cloutop entrainment instability. *Journal of the Atmospheric Sciences*, *37*, 131–147.
- Deardorff, J. W. (1970). Convective velocity and temperature scales for the unstable planetary boundary layer. *Journal of the Atmospheric Sciences*, *27*(8), 1211–1213. [https://doi.org/10.1175/1520-0469\(1970\)027<1211:CVATSF>2.0.CO;2](https://doi.org/10.1175/1520-0469(1970)027<1211:CVATSF>2.0.CO;2)
- Deardorff, J. W. (1976). On the entrainment rate of a stratocumulus-topped mixed layer. *Quarter Journal of the Royal Meteorological Society*, *102*(433), 563–582. <https://doi.org/10.1002/qj.49710243306>
- Deardorff, J. W., Willis, G. E., & Lilly, D. K. (1969). Laboratory investigation of non-steady penetrative convection. *Journal of Fluid Mechanics*, *35*(01), 7–31. <https://doi.org/10.1017/S0022112069000942>
- Deardorff, J. W., Willis, G. E., & Stockton, B. H. (1980). Laboratory studies of the entrainment zone of a convectively mixed layer. *Journal of Fluid Mechanics*, *100*(01), 41–64. <https://doi.org/10.1017/S0022112080001000>
- Farmer, D. M. (1975). Penetrative convection in the absence of mean shear. *Quarter Journal of the Royal Meteorological Society*, *101*(430), 869–891. <https://doi.org/10.1002/qj.49710143011>
- Fukao, S., Sato, T., Tsuda, T., Yamamoto, M., & Yamanaka, M. D. (1990). MU radar—New capabilities and system calibrations. *Radio Science*, *25*(4), 477–485. <https://doi.org/10.1029/RS025i004p00477>
- Galperin, B., Kantha, L. H., Hassid, S., & Rosati, A. (1988). A quasi-equilibrium turbulent energy model for geophysical flows. *Journal of the Atmospheric Science*, *45*(1), 55–62. [https://doi.org/10.1175/1520-0469\(1988\)045<0055:AQETEM>2.0.CO;2](https://doi.org/10.1175/1520-0469(1988)045<0055:AQETEM>2.0.CO;2)
- Glickman, T. (2000). *Glossary of meteorology*. MA, USA: American Meteorological Society.
- Kantha, L. (2003). On an improved model of the turbulent PBL. *Journal of the Atmospheric Sciences*, *60*(17), 2239–2246. [https://doi.org/10.1175/1520-0469\(2003\)060<2239:OAIMFT>2.0.CO;2](https://doi.org/10.1175/1520-0469(2003)060<2239:OAIMFT>2.0.CO;2)
- Kantha, L., & Carniel, S. (2009). A note on modeling mixing in stably stratified flows. *Journal of the Atmospheric Sciences*, *66*(8), 2501–2505. <https://doi.org/10.1175/2009JAS3041.1>
- Kantha, L., & Clayson, C. A. (2000). *Small Scale Processes in Geophysical Flows*. San Diego, CA: Academic Press
- Kantha, L., & Clayson, C. A. (2004). On the effect of surface gravity waves on mixing in the oceanic mixed layer. *Ocean Modeling*, *6*(2), 101–124. [https://doi.org/10.1016/S1463-5003\(02\)00062-8](https://doi.org/10.1016/S1463-5003(02)00062-8)
- Kantha, L., Lawrence, D., Luce, H., Hashiguchi, H., Tsuda, T., Wilson, R., et al. (2017). Shigaraki UAV-Radar Experiment (ShUREX): overview of the campaign with some preliminary results. *Progress in Earth and Planetary Science*, *4*, 19. <https://doi.org/10.1186/s40645-017-0133-x>
- Kantha, L. H. (1980). Turbulent entrainment at a buoyancy interface due to convective turbulence. In H. J. Freeland, D. M. Farmer, & C. D. Levings (Eds.), *Fjord oceanography* (pp. 205–214). New York, USA: Plenum Press.
- Kantha, L. H., & Clayson, C. A. (1994). An improved mixed layer model for geophysical applications. *Journal of Geophysical Research*, *99*(C12), 25,235–25, 266. <https://doi.org/10.1029/94JC02257>
- Kantha, L. H., & Mellor, G. L. (1989). A numerical model of the atmospheric boundary layer over a marginal ice zone. *Journal of Geophysical Research*, *94*(C4), 4959–4970. <https://doi.org/10.1029/JC094iC04p04959>
- Kantha, L. H., & Rosati, A. (1990). The effect of curvature on turbulence in stratified fluids. *Journal of Geophysical Research*, *95*(C11), 20,313–20,330. <https://doi.org/10.1029/JC095iC11p20313>
- Kudo, A. (2013). The generation of turbulence below midlevel cloud bases: The effect of cooling due to sublimation of snow. *Journal of Applied Meteorology*, *52*(4), 819–833. <https://doi.org/10.1175/JAMC-D-12-0232.1>
- Kudo, A., Luce, H., Hashiguchi, H., & Wilson, R. (2015). Convective instability underneath midlevel clouds: Comparisons between numerical simulations and VHF radar observations. *Journal of Applied Meteorology*, *54*, 2217–2227. <https://doi.org/10.1175/JAMC-D-15-0101.1>
- Lilly, D. K., & Schubert, W. H. (1979). The effects of radiative cooling in a cloud-topped mixed layer. *Journal of the Atmospheric Sciences*, *37*, 482–487.
- Luce, H., Hashiguchi, H., Kantha, L., Lawrence, D., Tsuda, T., Mixa, T., & Yabuki, M. (2018). On the performance of the range imaging technique estimated using unmanned aerial vehicles during the ShUREX 2015 campaign. *IEEE Transactions on Geoscience and Remote Sensing*, *56*(4), 2033–2042. <https://doi.org/10.1109/TGRS.2017.2772351>
- Luce, H., Nakamura, T., Yamamoto, M. K., Yamamoto, M., & Fukao, S. (2010). MU radar and lidar observations of clear-air turbulence underneath cirrus. *Monthly Weather Review*, *138*(2), 438–452. <https://doi.org/10.1175/2009MWR2927.1>
- Luce, H., Yamamoto, M., Fukao, S., Helal, D., & Crochet, M. (2001). A frequency domain radar interferometric imaging (FII) technique based on high-resolution methods. *Journal of Atmospheric and Solar-Terrestrial Physics*, *63*(2-3), 221–234. [https://doi.org/10.1016/S1364-6826\(00\)00147-4](https://doi.org/10.1016/S1364-6826(00)00147-4)

- Mellor, G., & Yamada, T. (1982). Development of a turbulence closure model for geophysical fluid problems. *Reviews of Geophysics and Space Physics*, 20(4), 851–875. <https://doi.org/10.1029/RG020i004p00851>
- Rosenfeld, D., & Mintz, Y. (1988). Evaporation of rain falling from convective clouds as derived from radar measurements. *Journal of Applied Meteorology*, 27(3), 209–215. [https://doi.org/10.1175/1520-0450\(1988\)027<0209:EORFFC>2.0.CO;2](https://doi.org/10.1175/1520-0450(1988)027<0209:EORFFC>2.0.CO;2)
- Stull, R. B. (1973). Inversion rise model based on penetrative convection. *Journal of the Atmospheric Sciences*, 30(6), 1092–1099. [https://doi.org/10.1175/1520-0469\(1973\)030<1092:IRMBOP>2.0.CO;2](https://doi.org/10.1175/1520-0469(1973)030<1092:IRMBOP>2.0.CO;2)
- Wang, Y., You, Y., & Kulie, M. (2018). Global virga precipitation distribution derived from three spaceborne radars and its contribution to the false radiometer precipitation detection. *Geophysical Research Letters*, 45, 4446–4455. <https://doi.org/10.1029/2018GL077891>
- Willis, G. E., & Deardorff, J. W. (1974). A laboratory model of the unstable planetary boundary layer. *Journal of the Atmospheric Sciences*, 31(5), 1297–1307. [https://doi.org/10.1175/1520-0469\(1974\)031<1297:ALMOTU>2.0.CO;2](https://doi.org/10.1175/1520-0469(1974)031<1297:ALMOTU>2.0.CO;2)
- Wilson, R., Luce, H., Hashiguchi, H., Nishi, N., & Yabuki, M. (2014). Energetics of persistent turbulent layers underneath mid-level clouds estimated from concurrent radar and radiosonde data. *Journal of Atmospheric and Solar - Terrestrial Physics*, 118, 78–89. <https://doi.org/10.1016/j.jastp.2014.01.005>
- Zhou, S., Zhai, X., & Renfrew, I. A. (2018). The impact of high-frequency weather systems on SST and surface mixed layer in the central Arabian Sea. *Journal of Geophysical Research: Oceans*, 123, 1091–1104. <https://doi.org/10.1002/2017JC013609>